8

The Wavelet Transform: A Method for Time-Frequency Localization

Ingrid Daubechies

8.1 INTRODUCTION

In this chapter we study the mathematical properties of two linear time-frequency analysis methods. The first is the familiar *windowed Fourier transform,*

$$c_{mn}(f) = \int_{-\infty}^{\infty} dt\ e^{2\pi j m \nu_0 t}\, g(t - nt_0)\, f(t), \tag{8.1}$$

and the second is the *wavelet transform,*

$$C_{mn}(f) = a_0^{-m/2} \int_{-\infty}^{\infty} dt\ h(a_0^{-m}t - nb_0)\, f(t). \tag{8.2}$$

In both cases the function f is characterized by a sequence of numbers labeled by $\mathbb{Z}^2$; the first index in c_{mn} or C_{mn} labels the frequency or scale information, the second index the instant in time around which the frequency decomposition is made. Transforms such as (8.1) or (8.2) give the frequency content of the function $f(t)$ *locally in time*. In this they are similar to music notation, which tells the music player the notes (= frequency information) to play at any given moment. The usual Fourier transform* (without a moving window),

$$F(\nu) = \int dt\, e^{2\pi j \nu t}\, f(t), \tag{8.3}$$

also gives the frequency content of $f(t)$, but information concerning time localization of, for example, high-frequency bursts cannot be read off easily from $F(\nu)$. In this sense, (8.3) lacks the time localization that both (8.1) and (8.2) possess.

The transforms (8.1) and (8.2) can be viewed as discretizations of the following "continuous" versions:

$$\phi_f(\nu, t) = \int_{-\infty}^{\infty} dt'\, e^{2\pi j \nu t'}\, g(t' - t)\, f(t') \tag{8.4}$$

and

$$\Phi_f(a, b) = a^{-1/2} \int_{-\infty}^{\infty} dt\, h\left(\frac{t-b}{a}\right) f(t), \tag{8.5}$$

corresponding to the *discrete lattices:*

$$\begin{aligned} &\nu = m\nu_0,\ t = nt_0 && \text{in the windowed Fourier transform case,} \\ &a = a_0^m,\ b = nb_0\, a_0^m && \text{in the wavelet case.} \end{aligned} \tag{8.6}$$

Note that (8.4) and (8.5) are *linear* in the signal $f(t)$, as opposed to another very useful time-localization method, the Wigner transform,† which is quadratic in f. Because of this linearity, *the windowed Fourier transform and the wavelet transform do not exhibit the interference patterns typical for the Wigner transform of most functions $f(t)$.* On the other hand, both (8.1) and (8.2) select a *window function* g or a *wavelet* h as the basic analyzing tool; no such basic function is built into the Wigner transform. Another difference is that the Wigner distribution is always real, whether the signal to be analyzed is real or complex. The windowed Fourier transform (8.4) is never a real function on the time-frequency plane, regardless of the choice of g, even for real signals $f(t)$. The wavelet transform (8.5) is real if the signal f is real and if the basic wavelet h is chosen to be real as well. In some applications it may, however, be useful to choose h complex, even for the analysis of real signals (see Section 8.3).

*In this chapter, we use the symbol $f(t)$ for denoting a time function, and the symbol $F(\nu)$ for denoting its Fourier transform, with ν denoting frequency.

†The Wigner distribution is discussed in detail in Chapter 9.

Here, we shall discuss in some detail the mathematical properties of both windowed Fourier transform and the wavelet transform. We start by making a qu itative comparison between the two transforms in Section 8.2. We show that by construction the wavelet transform is particularly well suited for signals with sh lived high-frequency phenomena superposed on much lower frequencies. In Sect 8.3 we study the continuous transforms (8.4) and (8.5). They have very easy inv sion formulas, also in the form of an integral transform. We show how these tra forms can be used to build a particular set of time-frequency filtering operators w explicit and easily computable eigenfunctions and eigenvalues. In Section 8.4 turn to the discrete transforms (8.1) and (8.2). Since there exist integral transfor inverting the continuous versions (8.4) and (8.5), it is to be expected that for s ficiently dense meshes of type (8.6), the discrete transforms have inverses as w This turns out to be true. For fairly general functions g or h, one can find pairs threshold values $\tilde{\nu}_0$, $\tilde{t}_0$ or $\tilde{a}_0$, $\tilde{b}_0$ such that there exists a numerically stable procedu to recover f from the coefficients $c_{mn}(f)$ or $C_{mn}(f)$, provided the mesh paramet are smaller than the threshold values. We also show that the resulting decompo tion + reconstruction procedure really provides time-frequency localization in t following sense: if f is essentially localized in the time interval $[-T, T]$ and its Four transform F is essentially localized in $[-\Omega, \Omega]$, then only those coefficients corr sponding to time-frequency points within or close to the region $[-T, T] \times [-\Omega,$ are needed to reconstruct f approximately. In many cases, the transforms (8.1) a (8.2) are "redundant": the functions $g_{mn}(t)$ $(m, n \in \mathbb{Z})$ or $h_{mn}(t)$ $(m, n \in$ where

$$g_{mn}(t) = e^{-2\pi j m \nu_0 t}\, g(t - nt_0)$$

and

$$h_{mn}(t) = a_0^{-m/2}\, h(a_0^{-m} t - nb_0)$$

are not linearly independent. For some applications, this is an advantage. In oth applications, we like to reduce this redundancy as much as possible. In Section 8 we discuss the extreme case, where the g_{mn} or h_{mn} constitute an orthonormal basi It turns out that in the windowed Fourier transform case, the associated functio g_{mn} can only constitute an orthonormal basis if g is badly localized in either time frequency. No such restriction holds for the wavelet transform case. There exi "nice" functions h such that the h_{mn} constitute an orthonormal basis for L^2 ($\mathbb{R}$ These orthonormal wavelet bases turn out to be related to a special class of filte used in subband coding. We shall give a few examples of orthonormal wavelet bas and briefly explain one application of them to image analysis.

The material presented in this chapter is a synthesis of several papers on th wavelet transform. The wavelet transform was first proposed as a tool for sign analysis by the geophysicist Morlet [1], [2]. The numerical success of Morlet's met od prompted Grossmann to make a detailed mathematical study of the wavelet tran form in its "continuous form" (8.5) [3], [4], [5]. This resulted in an inversion formul for (8.5) (based on the "resolution of the identity," see Section 8.3) and interpolation formulas [6]. The mathematical study of the discrete case started with the introduction of "frames" (see Section 8.4) in [7] and was carried out in greater detail in [8]. In the meantime orthonormal bases of wavelets were discovered (see Section 8.5). A first construction made by Stromberg [9] went unfortunately largely unnoticed. A few years later Y. Meyer constructed a different basis [10], which was extended to more than one dimension in [11]. Other bases, numerically more useful because they were more concentrated, were constructed by Lemarié [12] and Battle [13]. It was then realized by Mallat and Meyer that orthonormal bases of wavelets could be constructed systematically from a general framework called "multiresolution analysis," [14], [15]. This framework was applied by Mallat to vision analysis [16], [17]. It also provided the inspiration for the construction of compactly supported orthonormal wavelets in [18].

It is the goal of this chapter to present some of the flavor of these different and exciting results on wavelets. Wherever the techniques that we discuss can be applied to the windowed Fourier transform as well, we present the two cases in parallel, pointing out the analogies and the differences. In most cases we shall not go into the technical details of the proofs, which the interested reader can find in the references.

8.2 QUALITATIVE COMPARISON OF THE WINDOWED FOURIER TRANSFORM AND THE WAVELET TRANSFORM

To illustrate this comparison we give graphs of typical g_{mn} and h_{mn} in Fig. 8.1. We also show their corresponding time-frequency localization lattices in Fig. 8.2, representing each g_{mn} or h_{mn} by the points in time-frequency space around which that function is mostly concentrated. In the windowed Fourier transform case, assuming that $\int dt|g(t)|^2 = 1$, and $\int dt\, t|g(t)|^2 = 0 = \int d\nu\, \nu|G(\nu)|^2$, the lattice points are given by

$$(nq_0, mp_0) = [\int dt\ t|g_{mn}(t)|^2,\ \int d\nu\ \nu|G_{mn}(\nu)|^2].$$

In the wavelet case we again associate to every h_{mn} the space localization point $\int dt\ t|h_{mn}(t)|^2 = nb_0\, a_0^m$ (assuming that $\int dt|h(t)|^2 = 1$ and $\int dt\, t|h(t)|^2 = 0$). Since the function $|H|$, and consequently all the $|H_{mn}|$, is even in many applications, the choice $\int d\nu\ \nu|H_{mn}(\nu)|^2$ is not appropriate for the frequency localization, since this integral is zero. This is due to the fact that the H_{mn} have *two* peaks, one for positive and one for negative frequencies. We therefore represent the frequency content of h_{mn} by *two* points, namely, $\int_0^\infty d\nu\ \nu|H_{mn}(\nu)|^2$ and $\int_{-\infty}^0 d\nu\ \nu|H_{mn}(\nu)|^2$. The

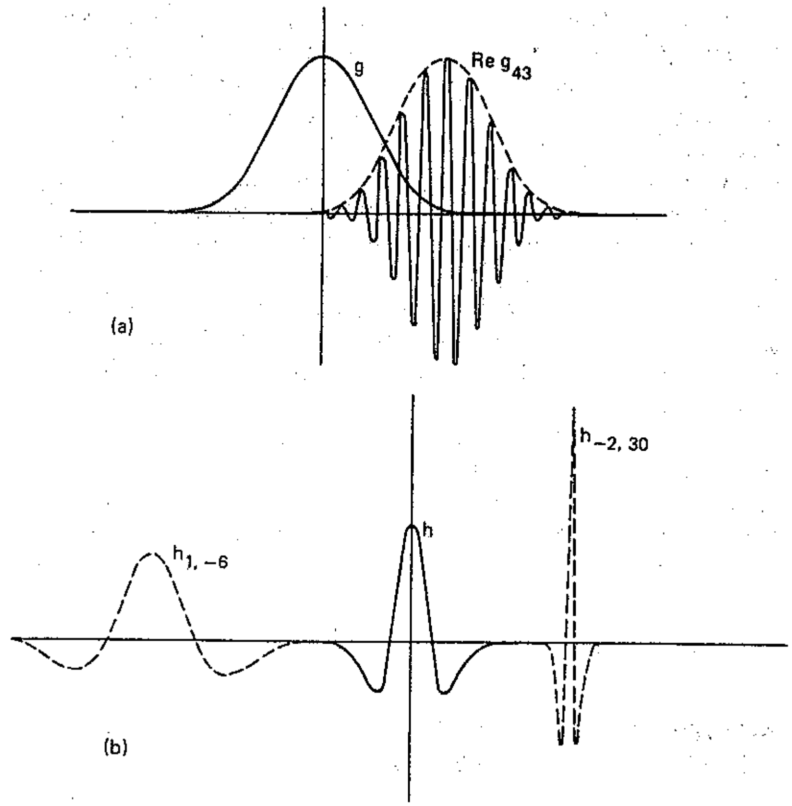

Figure 8.1 (a) A typical choice for the window function $g = g_{00}$ and a typical g_{mn}. In this case, $g(t) = \pi^{-1/4}\exp(-t^2/2)$, $\nu_0 = \pi$, $t_0 = 1$; the figure shows Re $g_{43}(t) = \pi^{-1/4}\cos(4\pi t)\exp[-(t-3)^2/2]$. (b) A typical choice for the basic wavelet $h = h_{00}$, and a few typical h_{mn}. In this case $h(t) = 2/\sqrt{3}\,\pi^{-1/4}(1-t^2)\exp(-t^2/2)$, $a_0 = 2$, $b_0 = 1$.

two lattice points corresponding to the positive and negative frequency locali: of h_{mn} are thus

$$(nb_0\, a_0^m,\, a_0^{-m}\,\omega_\pm) = \left(\int dt\; t|h_{mn}(t)|^2,\quad \int_{0 \le \pm\nu < \infty} d\nu\; \nu|H_{mn}(\nu)|^2\right),$$

where $\omega_\pm = \int_{0 \le \pm\nu < \infty} d\nu\; \nu|H(\nu)|^2$. Figure 8.1 shows one very basic differen tween the windowed Fourier transform and the wavelet transform: while the s the support of the g_{mn} is fixed, the support of the h_{mn} is essentially proportio a_0^m. As a result the h_{mn} corresponding to high frequencies, that is, with $m \ll$

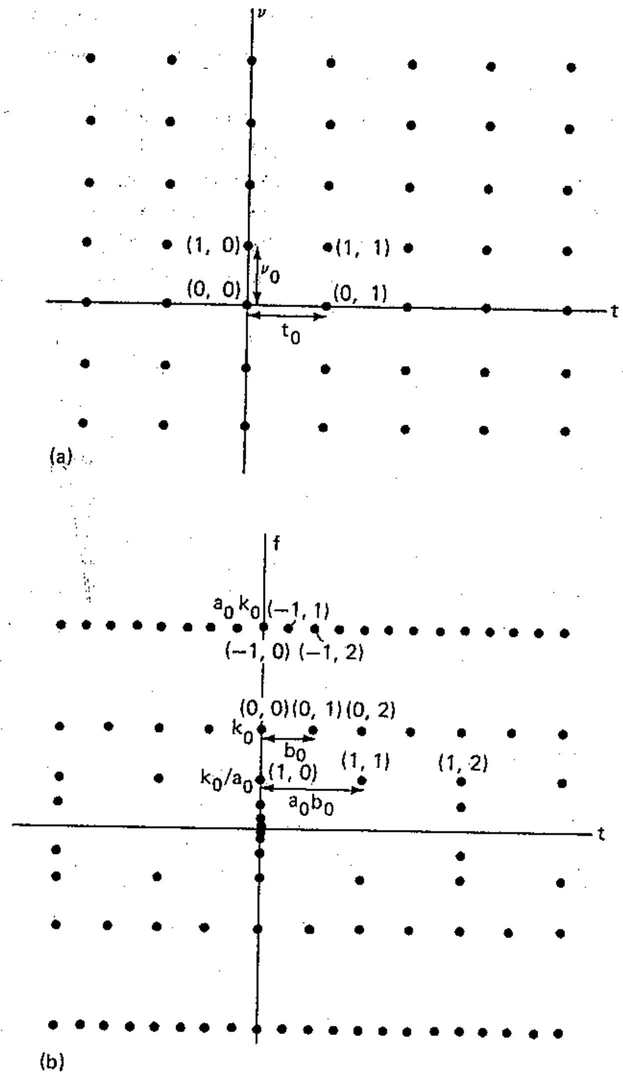

Figure 8.2 (a) The phase space lattice corresponding to the short-time Fourier transform (see text). (b) The phase space lattice corresponding to the wavelet transform (see text). The constant k_0 is given by $k_0 = \int_0^\infty d\nu\, \nu^{-1}|H(\nu)|^2$; we have assumed H to be even, and we have chosen $a_0 = 2$.

very much concentrated. This means of course that the time-translation step has to be smaller for high-frequency h_{mn}, as is borne out by the phase space lattice in Fig. 8.2(b). It also means, however, that the wavelet transform will be able to "zoom in" on singularities, using more and more concentrated h_{mn} corresponding to higher and higher frequencies.

We illustrate this by the following simple example, taken from a grossly simplified problem in the synthesis of music. Typically, we need to be able to handle relatively low frequencies, corresponding to the lowest notes, and very high frequencies, corresponding to high harmonics. Suppose we want to be able to represent tones with frequency of the order of $2\pi/T$. Suppose also that we want to be able to render faithfully the "attack" of notes. This "attack" consists of very high harmonics, at the start of the note, that die out very quickly, typically in a time $t_0 \ll T$. We have represented one component of such an "attack," very schematically, in Fig. 8.3. Intuitively, the function $f(t)$ in Fig. 8.3 seems to correspond to a signal with "frequency" $2\pi(3/t_0) = 6\pi/t_0$ during the time interval $[0, t_0]$, while its amplitude on $[t_0, T]$ is zero. Let us compare the performances of the windowed Fourier transform and the wavelet transform for this problem. In the first case, the support of g, and hence that of all the g_{mn}, needs to have a width of at least T. The high-frequency $6\pi/t_0$ corresponds to a value for m of more or less $6\pi t_0^{-1} p_0^{-1}$. In practice, however, since $T \gg t_0$, much higher values of m than $6\pi p_0^{-1} t_0^{-1}$ will be needed to reproduce, by means of the g_{mn} sketched in Figure 8.1(a) (and that all have width T), a function f which is nonzero only in the interval $[0, t_0]$. This is not the case if wavelets are used. The high-frequency wavelets have very small support, so that the foregoing problem (having to bring in much higher frequencies than intuitively needed) does not occur. Moreover, even for the high frequencies corresponding to f, which correspond, in the wavelet transform, to very negative values of m, and a very small time translation step (see Fig. 8.2(b)), only a few of the many time steps necessary to cover $[0, T]$ would be needed, namely only those corresponding to $[0, t_0]$. This is what is meant by the "zooming in" property of the wavelets. For this kind of problem, wavelets thus provide a more efficient way (needing fewer coefficients) for the representation of the signal.

The foregoing example is so much simplified that it is rather unrealistic. The "zooming-in" faculty of the wavelets, illustrated by this example, does however play an important role in more realistic applications. It makes the wavelets a useful tool in the areas of signal analysis where they have been or are being tried out. These include seismic analysis [2], [1] and music analysis and synthesis [19], [20]. This same property also makes the wavelets a choice tool for the detection of singularities [21],

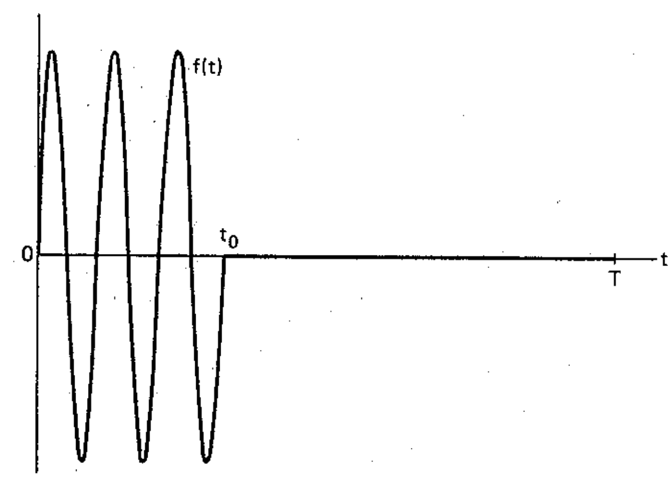

Figure 8.3 One component of the attack of a note (see text). We take, as a model,

$$f(t) = \begin{cases} \sin(6\pi t/t_0), & 0 \le t \le t_0 \\ 0, & t \le 0 \text{ or } t \ge t_0. \end{cases}$$

The lowest frequency of interest is $2\pi T^{-1}$; typically $t_0 << T$.

[22], which is of great interest to the analysis of vision [16], [14], [17], and for the study of fractals [23]. As a final remark we note that the wavelet transform, unlike the short-time Fourier transform, treats frequency in a logarithmic way (as clearly shown by Fig. 8.2), which is similar to our acoustic perception. This is another argument for the use of wavelets for the analysis and/or synthesis of acoustic signals.

8.3 THE CONTINUOUS TRANSFORMS

The mathematical aspects of the continuous versions of the windowed Fourier transform (8.4) and the wavelet transform (8.5) are very similar. We shall therefore discuss both transforms here. We start with the more familiar windowed Fourier transform.

8.3.1 The Windowed Fourier Transform: Continuous Version

Given a window function g, we define the windowed Fourier transform ϕ_f of a function $f(t)$ by

$$\phi_f(\nu, t) = \int_{-\infty}^{\infty} dt' \; e^{2\pi j \nu t'} \quad g(t' - t) \quad f(t').$$

The function ϕ_f can be considered as the scalar product of f with translated and modulated versions $g_{\nu,\, t}$ of the window function g:

$$\phi_f(\nu, t) = \langle g_{\nu,t}, f \rangle$$

with

$$g_{\nu,t}(s) = e^{-2\pi j \nu s} g(s - t).$$

Here we use the notation $\langle , \rangle$ for the standard L^2 scalar product, as shown by

$$\langle f, g \rangle = \int dx\, f^*(x)\, g(x),$$

where the asterisk denotes the complex conjugate. We shall denote the associated norm by $\|\ \|$,

$$\|f\| = \left[\int dx |f(x)|^2 \right]^{1/2}.$$

The window function g may be chosen arbitrarily in L^2 (R). In practice, we prefer of course window functions that are well concentrated in both time and frequency, so that $\phi_f(\nu, t)$ corresponds effectively to the "content" of f near time t and around frequency ν. A special choice is the Gaussian window,

$$g^0(t) = 2^{1/4}\, e^{-\pi t^2}; \tag{8.7}$$

the resulting $g^0_{\nu,t}$ are called *canonical coherent states* in the physics literature (see for example, [24]) or *Gabor wave functions* in the engineering literature (after Gabor [25]). The $g^0_{\nu,t}$ are localized, in time-frequency space, around (ν,t); that is,

$$\int ds\; s|g^0_{\nu,t}(s)|^2 = t$$

$$\int d\lambda\; \lambda|G^0_{\nu,t}(\lambda)|^2 = \nu,$$

where G denotes the Fourier transform of g as defined in (8.3).

The $g^0_{\nu,t}$ also minimize the uncertainty relation inequality:

$$[\int ds\, |g^0_{\nu,t}(s)|^2 (s-t)^2]\, [\int d\lambda |G^0_{\nu,t}(\lambda)|^2(\lambda-\nu)^2] = 1/(4\pi)^2.$$

In this sense the function $g^0_{\nu,t}$ is the L^2-function that achieves, of all L^2-functions, the best phase space localization around the phase space point (ν, t).

A very important, if not the most important, property of the functions $g_{\nu,t}$ is the *resolution of identity* [24]. This states that any function $f \in L^2(\mathbb{R}^n)$ can be reconstructed easily from the scalar products

$$\langle g_{\nu,t}, f\rangle = \int ds\; g^*_{\nu,t}(s)\, f(s).$$

One has indeed

$$\begin{aligned}
&\int d\nu \int dt\; g_{\nu,t}(s)\, \langle g_{\nu,t}, f\rangle \\
&= \int d\nu \int dt \int ds'\; e^{2\pi j\nu(s-s')}\, g(s-t)\, g^*(s'-t)\, f(s') \\
&= \int dt \int ds'\; \delta(s-s')\, g(s-t)\, g^*(s'-t)\, f(s') \\
&= f(s) \int dt|g(s-t)|^2 = f(s)\int dt|g(t)|^2.
\end{aligned}$$

If therefore g is normalized, that is, if $\int dt|g(t)|^2 = 1$, then we find that for all $f \in L^2(\mathbb{R}^n)$

$$f = \int d\nu \int dt\; g_{\nu,t}\langle g_{\nu,t}, f\rangle. \tag{8.8}$$

The "resolution of the identity," as given by (8.8), is valid for *any* choice of $g \in L^2(\mathbb{R}^n)$. However, if we make the "canonical chioce" $g = g^0$, then (8.8) has the following nice physical interpretation. For all phase space points (ν, t), we first project f onto the best localized function around (ν, t), by means of the operation

$$g^0_{\nu,t}\langle g^0_{\nu,t}, f\rangle;$$

integrating over all of phase space then regenerates f.

Remarks

1. Note that the map $f \to \phi(\nu, t) = \langle g_{\nu,t}, f \rangle$ sends a function of one variable into a function of two. This new function is square integrable,

$$\int d\nu \int dt |\phi(\nu, t)|^2 = \int dx |f(s)|^2 < \infty$$

(this immediately follows from (8.8)). There is of course a lot of redundancy in ϕ, and the range of this map is a subspace much smaller than $L^2(\mathbb{R}^2)$. For special choices of g, this subspace has been explicitly characterized. For $g = g^0$, for instance, we find that any such ϕ can be written in the form

$$\phi(\nu, t) = \exp\left[-\frac{1}{4}(\nu^2 + t^2) \right] \Psi(\nu + jt),$$

where Ψ is an entire analytic function on $\mathbb{C}^n$. Conversely, any square integrable ϕ of this form lies in the range of the map $f \to \phi$ (see [24] for more details, and for the original references).

2. The choice $g = g^0$ is special in more than one respect. Since $(g^0)^\wedge = g^0$, hence

$$G^0_{\nu,t}(\lambda) = e^{2\pi j\nu t} g_{-t,\nu}(\lambda),$$

we find

$$\langle g^0_{\nu,t}, f \rangle = e^{-2\pi j\nu t} \langle g^0_{-t,\nu}, \mathrm{F} \rangle.$$

This means that the windowed Fourier transforms of a function f and its Fourier transform F can be obtained from each other by a simple 90° rotation in time-frequency space (except for an unimportant phase factor).

It is now clear, from (8.8), that there exists a very easy inversion formula for the windowed Fourier transform:

$$f = \int d\nu \int dt\, g_{\nu,t}\, \phi_f(\nu, t), \tag{8.9}$$

or

$$f(s) = \int d\nu \int dt\, e^{-2\pi j\nu s}\, g(s - t)\, \phi_f(\nu, t). \tag{8.10}$$

Note that this is not the only inversion formula possible. This is because, as we pointed out, the ϕ_f only span a subspace of $L^2(\mathbb{R}^2)$. Formulas (8.9) or (8.10) provide, however, the "optimal" reconstruction. The same phenomenon will occur in the discrete "frame" case; see Section 8.4, where we shall give a more detailed discussion.

An interesting application of the above interpretation of formula (8.8) is the following construction of *time-frequency localization filters,* first presented in [26]. These "filters" are analogous to the band-limiting, time-limiting operators

$$(B_{W,T}f)(t) = \int_{-T}^{T} dt' \frac{\sin[W(t-t')]}{\pi(t-t')} f(t') \tag{8.11}$$

that effectively project f onto the time interval $[-T, T]$ and then project the Fourier transform of this restriction onto the frequency interval $[-W, W]$. The function $B_{W,T}f$ corresponds therefore to the "content" of f in the time-frequency region $[-T, T] \times [-W, W]$. The operators $B_{W,T}$ have been extensively studied [27], [28], [29]; their eigenfunctions are the *Slepian functions* or *prolate spheroidal wave functions,* used by D. Thomson in spectrum analysis [30]. Our interpretation of formula (8.8), as a projection onto the best possible localization around (ν, t), followed by an integration over ν, t to regenerate the original signal, allows us to construct "time-frequency localization operators" which are similar to but different from $B_{W,T}$. For any subset S of time-frequency space we define the localization operator P_S by

$$P_S f = \int_{(\nu,t)\in S} d\nu \int dt\; g^0_{\nu,t} \langle g^0_{\nu,t}, f\rangle. \tag{8.12}$$

These operators P_S are positive and bounded by 1,

$$\langle f, P_S f\rangle \geq 0, \qquad \|P_S f\| \leq \|f\|.$$

There is no restriction on the shape of S, apart from the fact that S should be measurable. This contrasts with the operators $B_{W,T}$ that focus on rectangles $[-T, T] \times [-W, W]$. Note that the cutoff defined by P_S is not "sharp" at the edges of S, in the sense that the function $P_S f$ will have some time-frequency content outside the set S, illustrated by $\langle g^0_{\nu',t'}, P_S f\rangle \neq 0$ for at least some $(\nu', t') \notin S$. Such a "tail" is unavoidable: for a bounded subset S of time-frequency space, no "sharp" localization operator (sharp in both time and frequency) exists. With our choice of the Gaussian window g^0 in (8.12), the tail of $P_S f$ outside f has very fast (Gaussian) decay, however.

For general sets S the operator P_S, as given by (8.12), is well defined, but its eigenfunctions and eigenvalues may be hard to characterize. In the special case where S has rotational symmetry in time-frequency space, things become much easier. In particular, if S is the disk S_R,

$$S_R = \{(\nu, t);\, \nu^2 + t^2 \leq R^2\},$$

then the eigenfunctions of P_{S_R} are *Hermite functions*, and the associated eigenvalues are given by *incomplete gamma-functions*,

$$P_{S_R} H_k = \lambda_k(R)\, H_k, \tag{8.13}$$

with

$$H_k(t) = 2^{1/4}\, \pi^{k/2}\, (k!)^{-1/2} \left(t - \frac{1}{2\pi}\frac{d}{dt}\right)^k e^{-\pi t^2}$$

$$\lambda_k(R) = \frac{1}{k!} \int_0^{\pi R^2} ds \; s^k \; e^{-s}.$$

This drastic simplification occurs when S has rotational symmetry because then P_S commutes with the second order differential operator $- d^2/dt^2 + 4\,\pi^2 t^2$; details can be found in [26]. Note that the R-dependence in (8.13) is completely concentrated in the eigenvalues $\lambda_k\,(R)$; the eigenfunctions H_k are independent of R. The eigenvalues $\lambda_k\,(R)$ are monotone decreasing functions of k (for fixed R); for small k, they are close to 1 and for large k they are close to zero. The "plunge" from 1 to 0 happens in an interval of width proportional to $\sqrt{R}$ around the threshold value $\pi\,R^2$ that is exactly the area of the time-frequency region S_R. All these features are reminiscent of what happens for the $B_{W,T}$ operators [29].

8.3.2 The Wavelet Transform: Continuous Version

Given a "basic wavelet" h, we define the wavelet transform Φ_f of a function $f(t)$ by

$$\Phi_f(a, b) = |a|^{-1/2} \int_{-\infty}^{\infty} dt\; h^*\left(\frac{t-b}{a}\right) f(t).$$

As in the windowed Fourier transform case, the function Φ_f can be considered as the scalar product of f with a two-parameter family of functions $h_{a,b}$:

$$\Phi_f(a,b) = \langle h_{a,b}, f\rangle$$

$$h_{a,b}(t) = |a|^{-1/2}\, h\left(\frac{t-b}{a}\right).$$

The parameter set for (a,b) is $(\mathbb{R}\backslash\{0\}) \times \mathbb{R}$. Again, there exists an associated "resolution of the identity". Its proof is as simple as in the windowed Fourier transform case:

$$\int_{-\infty}^{\infty} \frac{da}{a^2} \int_{-\infty}^{\infty} db\, \langle g, h_{a,b}\rangle \langle h_{a,b}, f\rangle$$

$$= \int_{-\infty}^{\infty} \frac{da}{a^2} \int_{-\infty}^{\infty} db \int_{-\infty}^{\infty} dy \int_{-\infty}^{\infty} dy'\; G^*(y)\, H_{a,b}(y)\, H^*_{a,b}(y')\, F(y')$$

$$= \int_{-\infty}^{\infty} \frac{da}{a^2} \int_{-\infty}^{\infty} db \int_{-\infty}^{\infty} dy \int_{-\infty}^{\infty} dy'\, e^{2\pi j b(y-y')}\, |a|\, H(ay)\, H^*(ay')\, G^*(y)\, F(y')$$

$$= \int_{-\infty}^{\infty} \frac{da}{|a|} \int_{-\infty}^{\infty} dy\, |H(ay)|^2 G^*(y)\, F(y)$$

$$= \left(\int_{-\infty}^{\infty} \frac{da}{|a|} |H(a)|^2 \right) \int_{-\infty}^{\infty} dy\, G^*(y)\, F(y) = C_b \langle g, f \rangle.$$

It follows, therefore, that

$$C_b^{-1} \int_{-\infty}^{\infty} \frac{da}{a^2} \int_{-\infty}^{\infty} db\, b_{a,b}\, \Phi_f(a,b) = f, \tag{8.14}$$

provided that

$$C_b = \int_{-\infty}^{\infty} dy\, |y|^{-1} |H(y)|^2 < \infty. \tag{8.15}$$

We shall only consider "admissible" wavelets, that is, functions b that satisfy the admissibility condition (8.15). If the function $b(t)$ decays at least as fast as $|t|^{-1-\epsilon}$ (in practice we shall assume much faster decay of b, to have good localization), then H is continuous, and (8.15) is equivalent to requiring that b has mean zero, as shown by

$$H(0) = \int_{-\infty}^{\infty} dy\, b(y) = 0.$$

For such admissible b, the resolution of the identity holds, and (8.14) provides a reconstruction formula for f from its wavelet transform Φ_f. The analogy between formulas (8.14) and (8.9) is no accident. In fact, both the widowed Fourier transform and the wavelet transform, in their continuous versions, are special cases of *square integrable group representations,* corresponding to the Weyl-Heisenberg group and the $ax + b$-group, respectively. It is typical for such representations to have a resolution of the identity. Details about this general framework, and its specialization to the two cases at hand, can be found in [6]. This reference also explains why (8.9) is true for any choice of the window function g, without restrictions on g, whereas (8.14) only holds for "admissible" wavelets b.

For special functions h, we can restrict the integration over a in (8.14) to positive values only. The derivation is entirely analogous, and (8.14) follows again, provided

$$\int_0^\infty dy\, |H(y)|^2 |y|^{-1} = \int_{-\infty}^0 dy\, |H(y)|^2 |y|^{-1} < \infty.$$

This is the case if, for example, $|H(-y)| = |H(y)|$. This is particularly so if h is a real function. The constant C_h has to be replaced by $\int_0^\infty dy\, |H(y)|^2 |y|^{-1}$ in this case.

Another variation arises if h is chosen so that H is a real function supported entirely on the positive half line $\mathbb{R}_+$. If the parameter a takes both positive and negative values, then we still find, even if support $H \subset [0, \infty)$,

$$\int_{-\infty}^{\infty} \frac{da}{a^2} \int_{-\infty}^{\infty} db\, h_{a,b}\, \Phi_f(a,b) = \left[\int_0^\infty dy\, y^{-1} |H(y)|^2\right] f. \tag{8.16}$$

We can however also restrict a to the positive half line; this is especially useful if the signal f is real. Rewrite the complex basic wavelet h as

$$h(t) = h_1(t) + jh_2(t),$$

where h_1, h_2 are real functions. Because support $H \subset [0, \infty)$, we find that h_2 is equal to the *Hilbert transform* of h_1, as shown by the frequency-domain relation:

$$H_2(\nu) = -j\, \mathrm{sgn}(\nu)\, H_1(\nu)$$

where sgn( ) is the *signum function*. Equivalently, we may write the time-domain relation:

$$h_2(t) = \frac{1}{2\pi} \lim_{\epsilon \to 0} \int_{|s| > \epsilon} ds\, \frac{1}{t - s}\, h_1(s).$$

We then find that

$$\int_0^\infty \frac{da}{a^2} \int_{-\infty}^{\infty} db\, [\langle g, (h_1)_{a,b}\rangle \langle (h_1)_{a,b}, f\rangle + \langle g, (h_2)_{a,b}\rangle \langle (h_2)_{a,b}, f\rangle]$$

$$= \int_0^\infty \frac{da}{a} \int_{-\infty}^{\infty} dy\, [|H_1(ay)|^2 + |H_2(ay)|^2]\, G^*(y)\, F(y)$$

$$= \left[\frac{1}{2}\int_0^\infty da\, a^{-1}|H(a)|^2\right] \langle g, f\rangle$$

which implies that

$$f = \left[\frac{1}{2}\int_0^\infty dy\, y^{-1}|H(y)|^2\right]^{-1} \int_0^\infty \frac{da}{a^2}\int_{-\infty}^\infty db\, [(b_1)_{a,b}\, \Phi_f^1(a,b) + (b_2)_{a,b}\, \Phi_f^2(a,b)].$$

For real functions f this can be rewritten as

$$f = \left[\frac{1}{2}\int_0^\infty dy\, y^{-1}|H(y)|^2\right]^{-1} \text{Re}\left[\int_0^\infty \frac{da}{a^2}\int_{-\infty}^\infty db\, b_{a,b}\, \Phi_f(a,b)\right].$$

A complex wavelet transform of this type can be very useful. The decomposition of the transform $\Phi_f(a,b)$ into its modulus and its phase is used intensively by Grossmann, Kronland-Martinet, and Morlet to detect small singularities in sound signals. Discontinuities in f or one of its derivatives (corresponding, for example, to a scratch on a record, or the addition of a higher harmonic in a chord) result in very striking patterns in the phase of $\Phi_f(a, b)$, with lines in the a,b-plane converging so as to pinpoint the exact time at which the discontinuity occurred. These patterns persist even if the signal is rather noisy. The interested reader should consult [31], [32], [22], and [19] for these and other applications.

Let us return to (8.16). This can be rewritten in a form that is even closer to (8.9). The time localization center of the $b_{a,b}$ is given by

$$\int_{-\infty}^\infty dt\, t|b_{a,b}(t)|^2 = b\int_{-\infty}^\infty dt|b(t)|^2 + \int_{-\infty}^\infty dt\, t|b(t)|^2$$
$$= b,$$

where we have assumed that b is normalized, $\int_{-\infty}^\infty dt|b(t)|^2 = 1$ and where we have used $b(-t) = b^*(t)$, since H is supposed to be real. The frequency localization is given by

$$\int_{-\infty}^\infty dy\, y|H_{a,b}(y)|^2 = \frac{1}{a}\int_0^\infty dy\, y|H(y)|^2.$$

We can therefore define the functions

$$\tilde{h}_{(\nu,t)}(s) = h_{\nu_1/\nu,t}(s) \tag{8.17}$$

with $\nu_1 = \int_0^\infty dy\, y|H(y)|^2$ and rewrite (8.16) as

$$f = \tilde{C}_h \int_{-\infty}^{\infty} d\nu \int_{-\infty}^{\infty} dt\, \tilde{h}_{(\nu,t)}\, \Psi_f(\nu, t), \tag{8.18}$$

where

$$\tilde{C}_h = \left[\int_0^\infty dy\, y|H(y)|^2\right]^{-1} \left[\int_0^\infty dy\, y^{-1}|H(y)|^2\right]^{-1}$$

and

$$\Psi_f(\nu, t) = \Phi_f\left(\frac{\nu_1}{\nu}, t\right).$$

Again (8.18) can be interpreted as an integral over all of time-frequency space of the time-frequency localized functions $\tilde{h}_{(\nu,t)}$, weighted by coefficients expressing the content of f near the time-frequency point (ν, t). The difference with (8.9) is that the building blocks $\tilde{h}_{(\nu,t)}$ are generated by dilations and translations, as shown by (8.17), resulting in better time resolution at high frequencies, as discussed in Section 8.2. If we restrict the integration in (8.18) to a subset S of the time-frequency plane, then this defines again a time-frequency localization operator P_S, as in the windowed Fourier case.

$$P_S f = \tilde{C}_h \int_{(\nu,t)\in S} d\nu \int dt\, \tilde{h}_{(\nu,t)}\, \Psi_f(\nu, t).$$

It turns out that there exist again special choices of h and S for which the eigenvalues and eigenfunctions of P_S can be given explicitly. These special sets are different from the disks in the windowed Fourier transform case; typically they cut off low as well as high frequencies, corresponding to a band-pass rather than a low-pass filter (see Fig. 8.4).

Details of this construction can be found in [33]. The shape of the domain in Fig. 8.4(b) can be changed by the choice of h; for every possible choice of h, its size can be changed as well (see Fig. 8.5). One example of a "good" h is the choice

$$H(y) = \begin{cases} 2y\, e^{-y} & y \geq 0 \\ 0 & y \leq 0 \end{cases}.$$

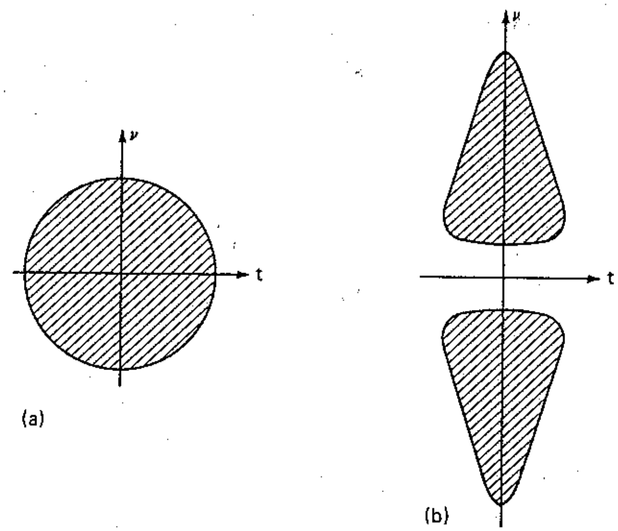

Figure 8.4 The difference between the explicit filters in the windowed Fourier transform case and the wavelet case. (a) Formula (8.12) leads to a simple time-frequency localization operator for disks in time-frequency space; (b) Formula (8.19) simplifies for special domains cutting off low and high frequencies.

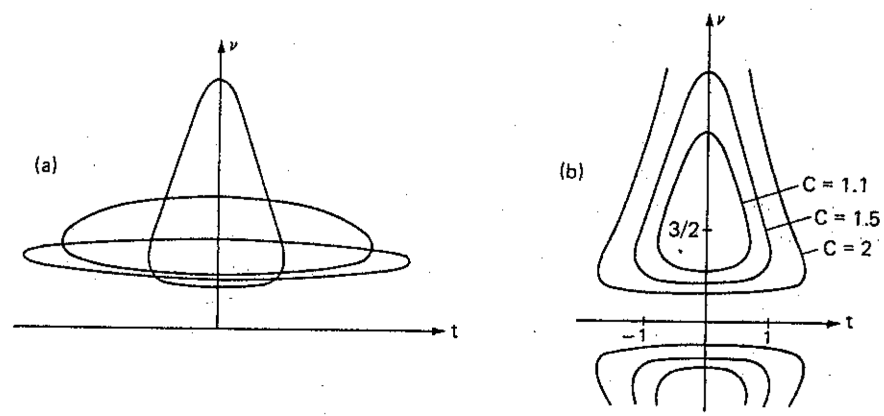

Figure 8.5 (a) Different shapes of S corresponding to different choices for b (see [34]). (b) The set S_c defined by (8.20) for different values of C.

The sets S for which P_s becomes particularly simple for this choice of b are

$$S_C = \left\{(\nu, t); \frac{(1 + t^2)\,\nu^2 + 9/4}{(3\nu)} \leq C\right\} \tag{8.20}$$

corresponding to values of a, b satisfying

$$(a - C)^2 + b^2 \leq C^2 - 1$$

or

$$a^2 + b^2 + 2aC + 1 \leq 0.$$

Here C can take any value ≥ 1. Figure 8.5b shows a few sets S_C corresponding to different values of C. The special role played by these particular sets S_C is again due to the fact that the P_{S_C} commute with a second-order differential operator (see [33]). The eigenfunctions of the P_{S_C} turn out to be Fourier transforms of Laguerre functions, and the associated eigenvalues are given by

$$\lambda_n(C) = (n+1)\left(\frac{C-1}{C+1}\right)^{n+1}\left(\frac{2}{C+1} + \frac{1}{n+1}\right).$$

8.4 THE DISCRETE TRANSFORMS: FRAMES

The resolutions of the identity (8.9) or (8.14) show that a signal f can be completely and easily reconstructed from either $\phi_f(\nu, t) = \langle g_{\nu,t}, f\rangle$ or $\Phi_f(a, b) = \langle h_{a,b}, f\rangle$, provided these transforms are known for all values of the parameters ν, t or a, b. In practice, however, the values of these parameters are restricted to discrete lattices, described in Section 8.1. It is not a priori obvious that f can be reconstructed from these discretized window Fourier transforms or wavelet transforms. We would expect that reconstruction is still possible if the discrete lattice has a very fine mesh, and is therefore very close to the continuous case; for very coarse meshes it seems clear that the coefficients will not contain enough information, rendering reconstruction impossible. This suggests the existence of threshold values for the lattice parameters. In what follows we shall introduce the concept of "frames," to study the existence of a numerically stable inversion procedure of the transforms (8.1) and (8.2). We start by some generalities concerning frames.

8.4.1 Frames

Frames were introduced by Duffin and Schaeffer [34] in a framework of nonharmonic Fourier analysis; see also [35]. Proofs for all the assertions in this subsection can be found in the original paper [34]; they are also reviewed in [8].

Let $(\phi_j)_{j\in J}$ be a set of elements of a Hilbert space $\mathcal{H}$. (In practice this set will be either $(g_{mn})_{m,n\in\mathbb{Z}}$ or $(h_{mn})_{m,n\in\mathbb{Z}}$, in $\mathcal{H} = L^2(\mathbb{R})$.) We shall call $(\phi_j)_{j\in J}$ a *frame* if there exist $A > 0$, $B < \infty$ such that, for all $j \in \mathcal{H}$,

$$A\|f\|^2 \leq \sum_{j\in J} |\langle\phi_j, f\rangle|^2 \leq B\|f\|^2. \tag{8.21}$$

We shall call A and B *frame bounds* for the frame $(\phi_j)_{j\in J}$. If $A = B$, that is, if

$$\sum_{j\in J} |\langle\phi_j, f\rangle|^2 = A\|f\|^2,$$

then we say that the $(\phi_j)_{j\in J}$ constitute a *tight frame*. If we define the linear operation T from $\mathcal{H}$ to $\ell^2(J)$, the square summable sequences indexed by J, by

$$(Tf)_j = \langle\phi_j, f\rangle, \tag{8.22}$$

then (8.21) ensures that

1. T is continuous: if f, f' are "close" (i.e., $\|f - f'\| \le \epsilon$), then the sequences Tf, Tf' will be "close" as well,

$$\|Tf - Tf'\|^2 = \sum_{j \in J} |\langle \phi_j, f \rangle - \langle \phi_j, f' \rangle|^2 \le B\,\epsilon^2$$

2. T is one-to-one: $Tf = Tf'$ implies $f = f'$.
3. T has a continuous inverse: if the sequences Tf and Tf' are close, then this means that f and f' were close in the first place, $\|f - f'\|^2 \le A^{-1}\|Tf - Tf'\|^2$.

Conversely, these three requirements imply (8.21). Note that although point 2 means that f can be characterized completely by the sequence of inner products $(\langle \phi_j, f \rangle)_{j \in J}$, the stronger requirement under 3 is needed for the existence of a numerically stable reconstruction algorithm for f from the $(\langle \phi_j, f \rangle)_{j \in J}$. We shall see below that the Gabor transform satisfies 2 but not 3, which explains why it suffers from numerical instabilities.

We shall call the operator T defined by (8.22) the "frame operator" of the frame $(\phi_j)_{j \in J}$. The adjoint operator T^* of T, from $\ell^2(J)$ to $\mathcal{H}$, is given by

$$T^* c = \sum_{j \in J} c_j\, \phi_j, \tag{8.23}$$

for any $c = (c_j)_{j \in J} \in \ell^2(J)$. Using the standard notation $T_1 \ge T_2$ for two operators T_1, T_2 if

$$\langle f, T_1 f \rangle \ge \langle f, T_2 f \rangle$$

for all $f \in \mathcal{H}$, we may easily check that (8.21) can be rewritten as

$$A\,\mathbf{1} \le T^* T \le B\,\mathbf{1}\,, \tag{8.24}$$

where $\mathbf{1}$ stands for the unit operator, $\mathbf{1}f = f$. Since $A > 0$, (8.24) implies that the operator $T^* T$ is invertible. Let us define

$$\tilde{\phi}_j = (T^* T)^{-1}\, \phi_j .$$

The $(\tilde{\phi}_j)_{j \in J}$ also constitute a frame, with frame bounds B^{-1}, A^{-1}. We shall call this the ***dual frame*** of $(\phi_j)_{j \in J}$. Moreover, we have

$$\begin{aligned} f &= (T^* T)^{-1}\,(T^* T) f \\ &= (T^* T)^{-1} \sum_{j \in J} (Tf)_j\, \phi_j \\ &= (T^* T)^{-1} \sum_{j \in J} \langle \phi_j, f \rangle\, \phi_j \\ &= \sum_{j \in J} \langle \phi_j, f \rangle\, \tilde{\phi}_j \end{aligned} \tag{8.25}$$

In the last equality we have commuted the sum over j with $(T^* T)^{-1}$; it is not hard to check that this is justified if (8.21) holds. Similarly one can show that

$$f = \sum_{j \in J} \langle \tilde{\phi}_j, f \rangle \, \phi_j. \tag{8.26}$$

Formulas (8.25) and (8.26) show dual aspects of the concept "frame." Formula (8.25) shows how to reconstruct f, given its inner products $\langle \phi_j, f \rangle$ with all the elements of a frame, whereas (8.26) indicates a way a computing the coefficients for an expansion of f with respect to the ϕ_j. We shall concentrate on the reconstruction of f from the $\langle \phi_j, f \rangle$, but it is important to bear in mind that all the results we present can be applied as well to expansions with respect to the ϕ_j.

Formulas (8.25) and (8.26) look very much like decompositions of $\mathcal{H}$ with respect to biorthogonal bases. It should be noted, however, that in general, frames are *not* bases: they contain "too many" vectors. Let us illustrate this by an example in the finite-dimensional space $\mathcal{H} = \mathbb{C}^2$. Define $\phi_1 = e_1$, $\phi_2 = -1/2 \ e_1 + \sqrt{3}/2 \ e_2$, $\phi_3 = -1/2 \, e_1 - \sqrt{3}/2 \, e_2$, where $e_1 = (1, 0)$ and $e_2 = (0, 1)$ constitute the standard basis for $\mathbb{C}^2$. We can easily check that, for all $v \in \mathbb{C}^2$,

$$\sum_{j=1}^{3} |\langle \phi_j, \mathrm{v} \rangle|^2 = \frac{3}{2} \|\mathrm{v}\|^2,$$

so that the $\{\phi_j; j = 1, 2, 3\}$ constitute a tight frame, with the inversion formula

$$\mathrm{v} = \frac{2}{3} \sum_{j=1}^{3} \phi_j \langle \phi_j, \mathrm{v} \rangle.$$

The $\{\phi_j; j = 1, 2, 3\}$ do not constitute a basis because they are not linearly independent. In the infinite-dimensional frames we shall consider in this chapter, any finite number of vectors will be linearly independent in general, but there will still be "too many" vectors in the sense that any of them lies in the closed linear span of all the others. Since the vectors constituting a frame are not linearly independent, it follows that (8.25) is not the only possible reconstruction formula for f from the coefficients $\langle \phi_j, f \rangle$: there exist other choices $\Psi_j \neq \tilde{\phi}_j$ such that

$$f = \sum_{j \in J} \langle \phi_j, f \rangle \, \Psi_j. \tag{8.27}$$

In the two-dimensional example we can take, for example, $\Psi_j = ⅔ \, \phi_j + a, j = 1, 2, 3$, where a is any vector in $\mathbb{C}^2$. The $\tilde{\phi}_j$ are however optimal in the sense that they are the *only* choice for which one automatically has

$$\sum_{j \in J} c_j \Psi_j = 0 \text{ if } \sum_{j \in J} c_j^* \langle \phi_j, f \rangle = 0, \qquad \text{for all } f \in \mathcal{H}.$$

This "optimality" of the $\tilde{\phi}_j$ means that if we attempt to apply the reconstruction formula (8.25) to a sequence $(c_j)_{j \in J}$ obtained from $\langle \phi_j, f \rangle_{j \in J}$ by some adulteration, as a result of roundoff or other errors, then the reconstruction automatically projects to zero any component in the sequence $(c_j)_{j \in J}$ that is orthogonal to the range of T. This does not happen with any other choice Ψ_j that satisfies (8.27).

This phenomenon occurs of course also for the dual formula (8.26). The linear dependence of the ϕ_j implies here that there exist other choices $c_j(f)$ such that

$$f = \sum_{j \in J} c_j(f)\, \phi_j. \tag{8.28}$$

We can however prove that for any such sequence of coefficients

$$\sum_{j \in J} |c_j(f)|^2 = \sum_{j \in J} |\langle \tilde{\phi}_j, f\rangle|^2 + \sum_{j \in J} |c_j(f) - \langle \tilde{\phi}_j, f\rangle|^2,$$

showing that the $\langle \tilde{\phi}_j, f\rangle$ have the minimal norm of all possible sequences satisfying (8.28).

In the case where the frame is tight, (8.25) and (8.26) simplify to

$$f = A^{-1} \sum_{j \in J} \langle \phi_j, f\rangle\, \phi_j. \tag{8.29}$$

If the frame is not tight, then the $\tilde{\phi}_j$ need to be computed before (8.25) or (8.26) can be used. From (8.24) we may construct a converging algorithm for the inversion of $T^* T$,

$$\begin{aligned} (T^* T)^{-1} &= \left\{ \frac{A+B}{2} \left[1 - \left(1 - \frac{2T^* T}{A+B} \right) \right] \right\}^{-1} \\ &= \frac{2}{A+B} \sum_{k=0}^{\infty} \left(1 - \frac{2T^* T}{A+B} \right)^k \end{aligned} \tag{8.30}$$

where the series converges because (use (8.24))

$$-\frac{B-A}{B+A} \le 1 - \frac{2T^* T}{A+B} \le \frac{B-A}{B+A},$$

hence

$$\left\| 1 - \frac{2T^* T}{A+B} \right\| \le \frac{B-A}{B+A} < 1.$$

The series (8.30) converges, therefore, at least as fast as the geometric series $\Sigma_k\, [(B-A)/(B+A)]^k$. It follows that it is advantageous to have frame bounds A, B that are close to each other. In many cases of practical interest, $(B-A)/(B+A) \cong BA^{-1} - 1$ is so small that only the first few terms of (8.30), or even only the first term, suffice to compute $\tilde{\phi}_j$ with sufficient precision,

$$\tilde{\phi}_j = \frac{2}{A+B} \phi_j + \frac{2}{A+B} \left[\phi_j - \frac{2}{A+B} \sum_{k \in J} \phi_k \langle \phi_k, \phi_j \rangle \right] + O([BA^{-1} - 1]^2)$$

$$= \frac{2}{A+B}\phi_j + O(BA^{-1} - 1).$$

Even if B/A is not very close to 1, then $\tilde{\phi}_j$ can still be computed by a simple iterative process,

$$\tilde{\phi}_j = \frac{2}{A+B} \lim_{k\to\infty} S_{k,j}$$

where

$$S_{0,j} = \phi_j$$

$$S_{k+1,j} = \phi_j + S_{k,j} - \frac{2}{A+B}\sum_{\ell\in J} \phi_\ell \langle \phi_\ell, S_{k,j}\rangle.$$

We are now ready to apply the frame concept to the windowed Fourier transform and the wavelet transform.

8.4.2 Frames and the Windowed Fourier Transform

As pointed out in the previous subsection, requiring that the $\langle g_{mn}, f\rangle$, with $g_{mn}(t) = e^{2\pi j m \nu_0 t} g(t - nt_0)$, can be used for a complete characterization and a stable reconstruction of f is equivalent to requiring that the $(g_{mn})_{m,n\in\mathbb{Z}}$ constitute a frame. In this subsection we shall see that for all practical purposes, this implies $\nu_0 t_0 < 1$. We shall also indicate how to find good estimates for A, B, and how to construct the dual frame $\tilde{g}_{mn}$. For $\nu_0 t_0 > 1$, there is no hope of even satisfying the basic requirements 1 and 2 of Section 8.4.1.

Theorem 4.1 *Let g be any element in $L^2(\mathbb{R})$. If $\nu_0 \cdot t_0 > 1$, then there exists $f \in L^2(\mathbb{R})$ such that $\langle g_{mn}, f\rangle = 0$ for all $m,n \in \mathbb{Z}$.*

In [27] an explicit construction of f is given for rational values of $\nu_0 \cdot t_0$. The theorem holds also for $\nu_0 \cdot t_0$ irrational, but the proof is more complicated (using von Neumann algebras) and nonconstructive. If g and its Fourier transform G decay faster than $(1+|x|)^{-(1+\epsilon)}$, then a beautiful and much simpler argument of Landau [36] shows that the g_{mn} cannot constitute a frame if $\nu_0 t_0 > 1$.

For the critical value $\nu_0 t_0 = 1$, we can find a function g such that the g_{mn} constitute a frame. For $\nu_0 = t_0 = 1$, an example is given by $g(t) = 1$ for $0 \le t \le 1$, $g(t) = 0$ otherwise. This function g is well localized in time, but its Fourier transform has very bad localization. The following theorem shows one cannot do much better.

Theorem 4.2 *Assume that*

$$\int_{-\infty}^{\infty} dt(1+t^2)|g(t)|^2 < \infty \quad \text{and} \quad \int_{-\infty}^{\infty} d\nu(1+\nu^2)|G(\nu)|^2 < \infty.$$

If $\nu_0 \cdot t_0 = 1$, then the g_{mn} do not constitute a frame.

This theorem was first stated by Balian [37] and Low [38], with the more narrow conclusion that the g_{mn} cannot be an orthonormal basis. A technical gap in their proof was filled by Coifman and Semmes, who also extended it to cover the frame case (see [8]). Subsequently, a beautiful simple proof for bases was found by Battle [39] and extended to frames in [40].

It follows that a frame with good localization in both time and frequency necessarily corresponds to $\nu_0 \cdot t_0 < 1$. The following theorem shows the advantages of a frame based on a function with good time-frequency localization.

Theorem 4.3 *Assume that*

$$|g(t)| \le C(1 + t^2)^{-\alpha}, \qquad |G(\nu)| \le C(1 + \nu^2)^{-\alpha},$$

for some $C > 0$, $\alpha > 1/2$. Then, for any $\epsilon > 0$, there exist t_ϵ, ν_ϵ such that, for all $f \in L^2(\mathbb{R})$ and for all $T, \Omega > 0$

$$\left\| f - \sum_{\substack{|m\nu_0| \le \Omega + \nu_\epsilon \\ |nt_0| \le T + t_\epsilon}} \tilde{g}_{mn} \langle g_{mn}, f \rangle \right\| \le (B/A)^{1/2} \left\{ \left[\int_{|\nu| \ge \Omega} d\nu |F(\nu)|^2 \right]^{1/2} + \left[\int_{|t| \ge T} dt |f(t)|^2 \right]^{1/2} + \epsilon \|f\| \right\}$$

The proof for this theorem can be found in [8]. The $\tilde{g}_{mn}$ are the elements of the dual frame of $(g_{mn})_{m,n \in \mathbb{Z}}$ (see also below).

Concretely, Theorem 4.3 means that if f is mostly concentrated in $[-T, T]$,

$$\int_{|t| \le T} dt |f(t)|^2 \ge (1 - \delta^2) \|f\|^2,$$

and if its Fourier transform is mostly concentrated in $[-\Omega, \Omega]$,

$$\int_{|\nu| \le \Omega} d\nu |F(\nu)|^2 \ge (1 - \delta^2) \|f\|^2,$$

then f can be reconstructed, up to an accuracy proportional to δ, by restricting the summation in the reconstruction formula (8.25) to only those lattice points $(m\nu_0, nt_0)$ within a neighborhood of the rectangle $[-\Omega, \Omega] \times [-T, T]$,

$$\left\| f - \sum_{\substack{|m\nu_0| \le \Omega + \nu(\delta) \\ |nt_0| \le T + t(\delta)}} \tilde{g}_{mn} \langle g_{mn}, f \rangle \right\| \le 3(B/A)^{1/2} \delta \|f\|.$$

This is the mathematical translation of the intuitive idea that the coefficients $\langle g_{mn}, f\rangle$ capture the "local" content of f near the time-frequency point $(m\nu_0, nt_0)$.

To reconstruct f from the $\langle g_{mn}, f\rangle$, we need to know the $\tilde{g}_{mn}$. In subsection 8.4.1 we showed how this dual frame can be computed by an iterative procedure. In principle, this procedure would have to be applied for every index $(m, n) \in \mathbb{Z}^2$. For the special case of frames associated to the windowed Fourier transform, a drastic simplification occurs. We have

$$
\begin{aligned}
& e^{2\pi j m\nu_0 t}(T^* T f)(t - nt_0) \\
&= e^{2\pi j m\nu_0 t} \sum_{k,l} g_{kl}(t - nt_0)\, \langle g_{kl}, f\rangle \\
&= \sum_{k,l} e^{-2\pi j k n \nu_0 t_0}\, g_{k+m,\, l+n}(t)\, \langle g_{kl}, f\rangle \\
&= \sum_{k,l} g_{kl}(t)\, \langle e^{-2\pi j k n\nu_0 t_0} g_{k-m,\, l-n}, f\rangle \\
&= \sum_{k,l} g_{kl}(t)\, \langle g_{kl}, e^{2\pi j m\nu_0 \cdot} f(\cdot - nt_0)\rangle.
\end{aligned}
$$

It follows that $T^* T$ commutes with multiplication by $e^{2\pi j m\nu_0 t}$ and translation by nt_0. Consequently $(T^* T)^{-1}$ also commutes with these two operations, so that

$$\tilde{g}_{mn}(t) = [(T^* T)^{-1} g_{mn}](t) = e^{2\pi j m\nu_0 t}\, [(T^* T)^{-1} g]\, (t - nt_0).$$

We therefore need to compute only one function $\tilde{g} = (T^* T)^{-1} g$.

Finally, it is useful to have good estimates for the frame bounds A and B; as was pointed out in Section 8.4.1, the iterative scheme for the computation of $\tilde{g}$ converges at least as fast as a geometric series in $(B/A) - 1$. For functions g with good time-frequency localization, surprisingly little work is needed to obtain such good estimates. If the translates $g(t - nt_0)$ don't have "gaps," in the sense that

$$\sum_n |g(t - nt_0)|^2 > 0, \qquad \text{for all } t,$$

and if g decays fast enough (e.g., faster than $(1 + |x|)^{-3}$, then the $g_{mn}(t) = e^{2\pi j m\nu_0 t} g(t - nt_0)$ constitute a frame for small enough ν_0, that is, for all ν_0 satisfying $0 < \nu_0 < \nu_0^{\text{thr.}}$ for some threshold value $\nu_0^{\text{thr.}}$ which can be explicitly computed. A proof of this assertion can be found in [8]; it uses the Poisson summation formula. The same argument can also be used to compute estimates for the frame bounds A and B [8]. These frame bounds necessarily satisfy [8]

$$A \leq (\nu_0 \cdot t_0)^{-1} \leq B. \tag{8.31}$$

In Table 8.1 we list our estimates for the frame bounds for $g(x) = 2^{1/4} \exp(-\pi x^2)$ and various choices of ν_0, t_0. For $\nu_0 \cdot t_0 = 1/4$ and $1/2$ we can also compute A and B exactly, via a different method. A comparison with these exact values shows that our estimates are pretty good (see [8].)

TABLE 8.1 Frame Bounds for $g(x) = 2^{1/4}\exp(-\pi x^2)$

$\nu_0 \cdot t_0 = 1/4$

t_0	A	B	B/A
0.4	24.229	24.234	1.00023
0.8	20.817	20.817	1.00000
1.2	8.884	8.884	1.00000
1.6	2.039	2.039	1.00000

$\nu_0 \cdot t_0 = 1/2$

t_0	A	B	B/A
0.4	3.815	3.820	1.00127
0.8	9.880	10.397	1.10691
1.2	4.437	4.447	1.00226
1.6	1.020	1.020	1.00001

$\nu_0 \cdot t_0 = 3/4$

t_0	A	B	B/A
0.4	0.175	0.180	1.02747
0.8	3.663	7.508	2.04959
1.2	2.453	3.470	1.41481
1.6	0.650	0.709	1.09123

$\nu_0 \cdot t_0 = .95$

t_0	A	B	B/A
0.4	0.0039	0.0087	2.20722
0.8	0.524	4.326	8.25997
1.2	0.515	4.161	8.08521
1.6	0.192	0.881	4.58378

Figure 8.6 shows the dual function $\tilde{g}$ for this same example, for different values of $\lambda = \nu_0 \cdot t_0$. In each case we have chosen $\nu_0 = t_0 = \sqrt{\lambda}$. For $\lambda = 1/4$, the function $\tilde{g}$ is virtually indistinguishable from a Gaussian, because A and B are very close together. As λ increases, several things happen: 1) both A and B decrease, so that $\tilde{g} = \dfrac{2}{A+B} g + O\left[\dfrac{B}{A} - 1\right]$ becomes larger; 2) the ratio B/A increases, so that the higher order terms in the expansion for $\tilde{g}$ become more important. This causes the deviation of $\tilde{g}$ from a Gaussian profile to become more marked. For $\lambda = 1$ the frame breaks down (as predicted by Theorem 2); the function $\tilde{g}$ can still be computed (via another method, see [41] [42]) but it is no longer a square integrable function.

8.4.3 Wavelet Frames

The machinery of Section 8.4.1 can also be applied to the wavelets

$$h_{mn}(t) = a_0^{-m/2}\, h(a_0^{-m} t - nb_0). \tag{8.32}$$

These wavelets can be considered as a "discretized" version of the continuously labeled families in Section 8.3.1. As a_0 tends to 1 and b_0 tends to 0, the discrete

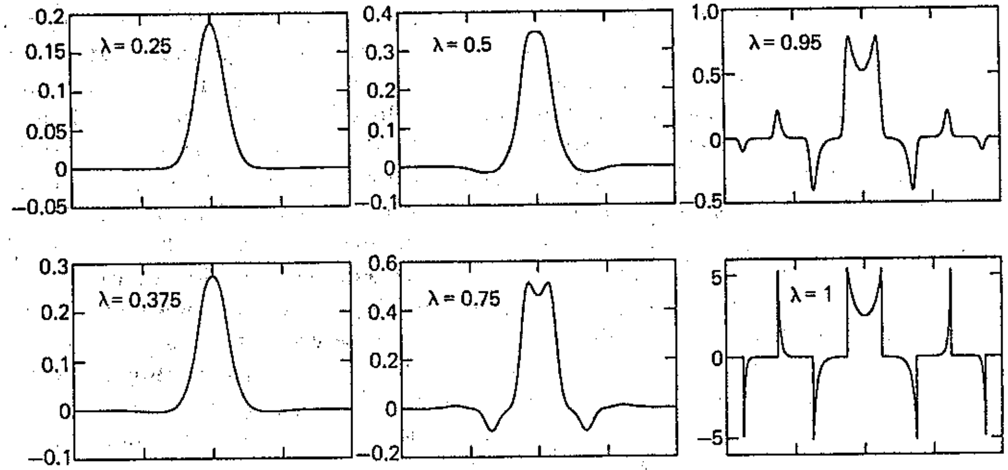

Figure 8.6 The dual function $\tilde{g}$ for the frames $g_{mn}(t) = 2^{1/4} \exp[2\pi j m v_o t - \pi(t - nt_o)^2]$, with $v_0 = t_0 = \sqrt{\lambda}$, for the values $\lambda = 0.25, 0.375, 0.5, 0.75$, and 0.95. For $\lambda = 1$, the dual function $\tilde{g}$ is no longer in $L^2(\mathbb{R})$.

family approaches, at least intuitively, a continuous family, and we may expect that only wavelets h that satisfy the admissibility condition (8.15) can give rise to frames with nondiverging frame bounds ($0 < A < B < \infty$). It turns out that this intuition is right. We can show that a family of wavelets $(h_{mn})_{m,n\epsilon z}$ as defined by (8.32) can only be a frame if the function h satisfies (8.15); the frame bounds are then constrained by the inequalities

$$A \leq \frac{\pi}{b_0 \log a_0} \int dy |y|^{-1} |H(y)|^2 \leq B. \tag{8.33}$$

Nonadmissible h lead to a diverging upper bound, that is, $B = \infty$. The inequalities (8.33) hold for *any* choices of a_0, b_0 (see [8]).

As in the continuous case, we can choose to work with wavelets that have positive frequencies only, support $H \subset [0, \infty)$. In this case, the frame uses the two functions h_+ and h_-, with $h_+ = h$ and $H_-(y) = H(-y)$, and the inequality (8.33) has to be adapted (see [8]). If only real signals f are analyzed, we may restrict our attention to only h_+ (see Section 8.3.2).

There are some crucial differences between wavelet frames and frames in the windowed Fourier transform situation. For instance, there exists no absolute, a priori limitation on a_0, b_0-values leading to frames. In fact, we can build a tight frame of wavelets for any pair (a_0, b_0) [7]. This freedom in the choice of a_0, b_0 is deceptive, however, because of the behavior of frames under dilations. If the h_{mn}, based on h, with parameters a_0, b_0, constitute a frame, then so do the $h_{\gamma;\,mn}$, based on $h_\gamma(x) = \gamma^{1/2} h(\gamma x)$, with frame parameters a_0, $\gamma^{-1} b_0$. This explains, at least partially, why a frame can be constructed for *any* pair a_0, b_0. To eliminate this dilational freedom, let us restrict our attention, in the present discussion, to frames such that $\|h\| = 1$ and $\int dy|y|^{-1}|H(y)|^2 = 1$. Under this restriction, we might hope again that there exists a critical curve $b_0^c(a_0)$ separating the "frameable" pairs from the "nonframeable," with the orthogonal bases corresponding to the curve itself. This is the situation for the windowed Fourier transform case: a family $(g_{mn})_{m,n\varepsilon\mathbb{Z}}$ can only constitute an orthonormal basis if $\nu_0\, t_0 = 1$ (we'll come back to this in Section 8.5); for $\nu_0\, t_0 > 1$, the g_{mn} cannot span all of $L^2(\mathbb{R})$ (see Theorem 4.1), and redundant sets correspond to $\nu_0\, t_0 < 1$. It turns out however that this picture is not true in the wavelet case. In [8] the following counterexample is established. We consider a basic wavelet ψ, constructed by Y. Meyer [10], and look at the $\psi_{mn;\, b_0}$, a family of wavelets generated from ψ with $a_0 = 2$, b_0 arbitrary. For $b_0 = 1$, these wavelets constitute an orthonormal basis [10]. If there existed a nice critical curve $b_0^c(a_0)$ separating frameable and nonframeable values, then we would expect that the $\psi_{mn;\, b_0}$ would not be a frame for $b_0 > 1$ ("not enough" vectors) and might be a frame consisting of nonindependent vectors for $b_0 < 1$ ("too many" vectors). It turns out, however (see [8]), that there exists $\varepsilon > 0$ such that, for all values of b_0 in $(1 - \varepsilon, 1 + \varepsilon)$, the associated $\psi_{mn;b_0}$ constitute a basis for $L^2(\mathbb{R})$. This baffling fact shows that the concept "time-frequency density," so well suited for the windowed Fourier transform, is not well adapted to the wavelet situation.

This example shows that there exist no straightforward analogs of Theorems 4.1 and 4.2 for the wavelet case. The localization expressed by Theorem 4.3 does have an analog, however.

Theorem 4.4 *Suppose that the $h_{mn}(x) = a_0^{-m/2}\, h(a_0^{-m} x - nb_0)$ constitute a frame, with frame bounds A, B, and dual frame $(h_{mn})^{\tilde{}}$. Assume that*

$$|H(y)| \le C|y|^{\beta}\,(1 + y^2)^{-(\alpha + \beta)/2},$$

where $\beta > 0$, $\alpha > 1$, and that, for some $\gamma > 1/2$

$$\int dx\,(1 + x^2)^{\gamma}|h(x)|^2 < \infty.$$

Fix $T > 0$, $0 < \Omega_0 < \Omega_1$. Then, for any $\varepsilon > 0$, there exists a finite subset $\mathcal{B}_\varepsilon(T, \Omega_1, \Omega_2)$ of $\mathbb{Z}^2$ such that, for all $f \in L^2(\mathbb{R})$,

$$\Big\| f - \sum_{(m,n)\,\varepsilon\,\mathcal{B}_\varepsilon(T,\Omega_1,\Omega_2)} (h_{mn})^{\tilde{}}\,\langle h_{mn}, f\rangle \Big\|$$

$$\le (B/A)^{1/2}\left\{\left[\int_{|t| \ge T} dt|f(t)|^2\right]^{1/2} + \left[\int_{\substack{|\omega| \le \Omega_0 \\ \text{or } |\omega| \ge \Omega_1}} d\omega|F(\omega)|^2\right]^{1/2} + \varepsilon\|f\|\right\}.$$

Figure 8.7 gives a schematic representation of such an "enlarged" set $\mathcal{B}_\varepsilon(T, \Omega_1, \Omega_2)$.

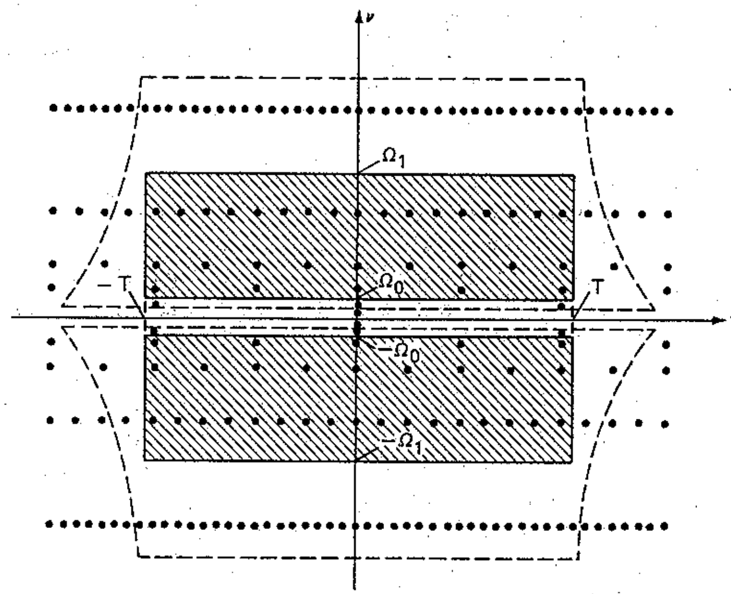

Figure 8.7 The lattice $(nb_0\, a_0^m, \pm a_0^{-m} k_0)$, indicating the localization of the h_{mn} [see Fig. 8.2(b)], and the two rectangles $[-T, T] \times [\Omega_0, \Omega_1]$, $[-T,T]$, $\times [-\Omega_1, -\Omega_0]$ on which the signal f is mainly concentrated. The coefficients $\langle h_{mn}, f \rangle$ corresponding to lattice points within the set $\mathcal{B}_\epsilon$ (in dashed lines) suffice to reconstruct f up to an error proportional to ϵ.

To apply formula (8.25) to wavelet frames, we need to compute the $\tilde{h}_{mn}$. We may easily check that T^*T, and therefore $(T^*T)^{-1}$, commutes with the dilations D_m,

$$(D_m f)(t) = a_0^{-m/2} f(a_0^{-m}\, t).$$

It follows that

$$\tilde{h}_{mn}(t) = a_0^{-m/2} \tilde{h}_{0n}(a_0^{-m}\, t),$$

reducing the number of different functions to be computed. Since T^*T does *not* commute with the translations by $a_0^m\, nb_0$, the $\tilde{h}_{0n}$ can in general not be obtained by translating a single function. In many applications, however, we like to use frames that are almost tight (see Table 8.2), in which case (see Section 8.4.1)

$$\tilde{h}_{mn}(t) \approx \frac{2}{A + B} h_{mn}(t).$$

Moreover, there exist special choices of h for which the dual frame is again generated by translations and dilations of a single function. This is the case for the orthonormal bases that we shall discuss in Section 8.5, where $\tilde{h}_{mn} = h_{mn}$, and for the nonorthonormal bases constructed by Tchamitchian in [43]. By introducing more redundancy, we can easily construct frames based on these bases, which still have the property that

$$\tilde{h}_{mn}(t) = a_0^{-m/2}\, \tilde{h}(a_0^{-m}t - nb_0)$$

for a suitable $\tilde{h}$.

As in the windowed Fourier transform case, we can show that for most "reasonable" wavelets h (that is, h that satisfy the admissibility condition (8.15), with at least some decay for h and H, and without big "gaps" in the family of functions $H(a_0^m y)$), there exist threshold values of a_0, b_0, so that choices of a_0, b_0 smaller than these threshold values lead to frames. Good estimates of the frame bounds can again be obtained via the Poisson summation formula [81]. Table 8.2 lists the frame bounds A, B for a few values of a_0, b_0 for the "Mexican hat function" $h(t) = 2/\sqrt{3}\ \pi^{-1/4}(1 - t^2)e^{-t^2/2}$. The parameter N indicates the number of "voices." These are introduced to obtain good frame bounds, while still working with a fixed dilation step $a_0 = 2$. Good, tight frame bounds can also be obtained by choosing smaller values for a_0; for practical implementation, however, $a_0 = 2$ is much more efficient. We may therefore choose to use several basic wavelets h^j, corresponding to different "voices," that is, having slightly different frequency ranges. The frame then consists

TABLE 8.2 Frame bounds for wavelet frames based on the Mexican hat function $h(t) = 2/\sqrt{3}\ \pi^{-1/4}(1 - t^2)e^{-t^2/2}$. The dilation parameter $a_0 = 2$ in all cases; N is the number of voices (see text).

$N = 1$

b_0	A	B	B/A
0.25	13.091	14.183	1.083
0.50	6.546	7.092	1.083
0.75	4.364	4.728	1.083
1.00	3.223	3.596	1.116
1.25	2.001	3.454	1.726
1.50	0.325	4.221	12.986

$N = 2$

b_0	A	B	B/A
0.25	27.273	27.278	1.0002
0.50	13.637	13.639	1.0002
0.75	9.091	9.093	1.0002
1.00	6.768	6.870	1.015
1.25	4.834	6.077	1.257
1.50	2.609	6.483	2.485
1.75	0.517	7.276	14.061

$N = 3$

b_0	A	B	B/A
0.25	40.914	40.914	1.0000
0.50	20.457	20.457	1.0000
0.75	13.638	13.638	1.0000
1.00	10.178	10.279	1.010
1.25	7.530	8.835	1.173
1.50	4.629	9.009	1.947
1.75	1.747	9.942	5.691

$N = 4$

b_0	A	B	B/A
0.25	54.552	54.552	1.0000
0.50	27.276	27.276	1.0000
0.75	18.184	18.184	1.0000
1.00	13.586	13.690	1.007
1.25	10.205	11.616	1.138
1.50	6.594	11.590	1.758
1.75	2.928	12.659	4.324

of $(h^j_{mn})m,n \in \mathbb{Z}; j = 0, \ldots, N-1$, where N is the number of voices. In practice, we often choose

$$h^j(t) = 2^{-j/N}\, h(2^{-j/N}\, t),$$

see [19], [22]. The computation of frame bounds for these frames is entirely analogous to the case $N = 1$ (see [8]).

Finally, we'd like to remark that very special wavelets h have been developed for which the decomposition of a (sampled) function into its wavelet component can be carried out very fast, in a number of steps proportional to the number of samples (and thus faster than an FFT!). This construction can be found in [44].

8.4.4 An Advantage of Redundant Frames: Less Precision on the Coefficients is Required

Morlet noticed, some time ago, that in numerical wavelet calculations, it often sufficed to calculate the wavelet coefficients to a precision of, say, 10^{-2}, in order to be able to reconstruct the original signal with a precision of, say, 10^{-3}. This rather surprising fact can be explained as a consequence of both phase space localization, and "oversampling."

Time-frequency localization is necessary to restrict oneself to a finite number of coefficients. We cannot hope to control an infinite number of coefficients if they can all induce an error of the same order. The role of "oversampling" is the following. Let us go back to the frame operator T defined in Section 8.4.1:

$$T: L^2(\mathbb{R}) \to \ell^2(\mathbb{Z}^2)$$
$$(Tf)_{m,n} = \langle \phi_{mn}, f \rangle,$$

where ϕ_{mn} stands for either h_{mn} or g_{mn}. Since the ϕ_{mn} constitute a frame, this operator is bounded and has a bounded inverse on its closed range. The operator T is onto (that is, Range $T = \ell^2(\mathbb{Z}^2)$) if and only if the ϕ_{mn} constitute a basis. In general, however, the ϕ_{mn} are not independent, and Range T is a proper subspace of $\ell^2(\mathbb{Z}^2)$. The inversion procedure,

$$f = \sum_{m,n} (\phi_{mn})^{\sim} \langle \phi_{mn}, f \rangle,$$

when applied to elements c of $\ell^2(\mathbb{Z}^2)$ not necessarily in Range T,

$$\sum_{m,n} (\phi_{mn})^{\sim}\, c_{mn},$$

consists in fact of (1) a projection of $\ell^2(\mathbb{Z}^2)$ onto Range T and (2) the inversion of T on its range (as discussed in Section 8.4.1). We shall model the finite precision of numerical calculations by adding random "noise" to the coefficients $\langle \phi_{mn}, f \rangle$, thus leading to modified coefficients $c_{mn}(f)$. The "noise" component of these coefficients "lives" on all of $\ell^2(\mathbb{Z}^2)$. If we apply the inversion procedure, this component will therefore be reduced in norm by the projection onto Range T. This reduction will be the more pronounced the "smaller" Range T is, as a subspace of $\ell^2(\mathbb{Z}^2)$, that is, the more pronounced the oversampling or redundancy in the frame. The calculations in the sequel show how this works in practice.

Let us assume that we are interested in signals f that are essentially localized in the time interval $[-T, T]$, and in the frequency range $[-\Omega, \Omega]$ (in the Weyl-Heisenberg case) or $[-\Omega_1, -\Omega_0] \cup [\Omega_0, \Omega_1]$ (in the wavelet case); that is,

$$\int_{|t| \geq T} |f(t)|^2 \leq \varepsilon^2 \|f\|^2$$

and

$$\int_{|\omega| \geq \Omega} |F(\omega)|^2 d\omega \leq \varepsilon^2 \|f\|^2$$

or

$$\left[\int_{|\omega| \geq \Omega_1} d\omega + \int_{|\omega| \leq \Omega_0} d\omega \right] |f(\omega)|^2 \leq \varepsilon^2 \|f\|^2.$$

Then, by Theorems 3 and 4, there exists an "enlarged box" $\mathcal{B}_\varepsilon$ such that

$$\left\| f - \sum_{(m,n) \in B_\varepsilon} (\phi_{mn})^{\sim} \langle \phi_{mn}, f \rangle \right\| \leq 3(B/A)^{1/2} \varepsilon |f|,$$

where ϕ denotes either g or h. Since $\mathcal{B}_\varepsilon$ is a finite subset of $\mathbb{Z}^2$, we restrict ourselves therefore to the finitely many coefficients $\langle \phi_{mn}, f \rangle$.

In practical calculations, the coefficients $\langle \phi_{mn}, f \rangle$ will be computed with finite precision. Let us take the following model for the errors. Assume that the coefficients to be used in the calculations are given by

$$\alpha_{mn}(f) = \langle \phi_{mn}, f \rangle + \gamma_{mn},$$

where the γ_{mn} are identical independently distributed random variables, with mean zero, and with variance δ^2:

$$\mathbb{E}\{\gamma_{mn}^2\} = \delta^2.$$

This means that the $\langle \phi_{mn}, f \rangle$ are known with "precision" δ. Note that our model is only a first approximation. In general the ϕ_{mn}, and hence the $\langle \phi_{mn}, f \rangle$, are not linearly independent, which means that the roundoff errors should not be regarded as independent random variables. With the above approximation, we find that the estimated error between f and a partial reconstruction, using only the finitely many coefficients associated to $(m,n) \in \mathcal{B}_\varepsilon$, and even those only with finite precision (i.e., replace $\langle\phi_{mn}, f\rangle$ by $\alpha_{mn}(f)$), is given by

$$\mathbb{E}\left\{\left\|f - \sum_{(m,n)\in\mathcal{B}_\varepsilon} \alpha_{mn}(f)\,(\phi_{mn})^{\sim}\right\|^2\right\}$$

$$= \mathbb{E}\left\{\left\|\left(f - \sum_{(m,n)\in\mathcal{B}_\varepsilon} (\phi_{mn})^{\sim}\langle\phi_{mn}, f\rangle\right) - \sum_{(m,n)\in\mathcal{B}_\varepsilon} \gamma_{mn}(\phi_{mn})^{\sim}\right\|^2\right\} \tag{8.34}$$

$$\leq 9(B/A)\,\varepsilon^2|f|^2 + A^{-2}\delta^2 N_\varepsilon,$$

where $N_\varepsilon = \#\mathcal{B}_\varepsilon$ and where we have used $\mathbb{E}(\gamma_{mn}) = 0$, $\mathbb{E}(\gamma_{mn}\gamma_{m'n'}) = \delta_{mm'}\delta_{nn'}\delta^2$, and $|(\phi_{mn})^{\sim}|^2 = |(T^*T)^{-1}\phi_{mn}|^2 \leq A^{-2}|\phi_{mn}|^2 = A^{-2}$.

The "reduction of calculational noise," observed by Morlet, is contained in the second term in (8.34), more particularly in the factor $N_\varepsilon A^{-2}$. Let us show how.

Assume that we are considering a Weyl-Heisenberg frame, g_{mn}, with $B \approx A$. If we assume that $\mathcal{B}_\varepsilon$ is large with respect to the lattice mesh, then (see Theorem 3)

$$N_\varepsilon = \#\mathcal{B}_\varepsilon \simeq \frac{4T\Omega}{\nu_0 \cdot t_0}.$$

On the other hand, if the frame is almost tight (i.e., $B \simeq A$), we find, by (8.31),

$$A \simeq (\nu_0 \cdot t_0)^{-1}$$

(we assume $\|g\| = 1$). Hence

$$N_\varepsilon A^{-2} \simeq 4T\Omega\,(\nu_0 \cdot t_0). \tag{8.35}$$

If the g_{mn} had constituted an orthonormal basis, then (provided we neglect the loss in phase space localization due to the use of an orthonormal basis) this factor would have been

$$(N_\varepsilon A^{-2})_{\text{orthon. basis}} \simeq 4T\Omega. \tag{8.36}$$

The frame gives thus a net gain of $(\nu_0 \cdot t_0)^{-1}$ with respect to the orthonormal basis situation.

Something similar happens for wavelets. In this case we don't have such a simple expression for N_ε, but we can easily see that the same phenomenon takes place by the following argument. Suppose b, a_0, b_0 are chosen so that the frame is almost tight, $A \simeq B$. Consider now the frame with the same b, a_0, but with $b_0' = b_0/2$. This frame will obviously also be close to tight, with $A' \approx B' \simeq 2A$. On the other hand, there are twice as many points in the graphical representation of this new frame for every frequency level. Hence $N_\varepsilon' = 2N_\varepsilon$. Combining these two, we find $N_\varepsilon' A'^{-2} = \tfrac{1}{2}N_\varepsilon A^{-2}$, that is, halving b_0 leads to a gain of 2 in the total error on f, for the same precision on the coefficients.

For the frames used by Morlet when he noticed this phenomenon, which were heavily oversampled (for example, he used up to 15 "voices") a gain factor of 10 or more can be obtained easily. Note, however, that oversampling does not explain completely the observed calculational noise (or quantization noise) reduction. As in vision analysis [16], part of the reduction is a consequence of the fact that, unlike the original signal, the coefficients $c_{mn}(f)$ at every fixed m-level are distributed around zero, with a sharp peak at zero. This apparently makes it possible to reduce drastically the number of quantization steps in the c_{mn}, without significantly altering the quality of the reconstructed signal [16].

8.5 ORTHONORMAL BASES

The frames studied in the previous section are usually redundant, in the sense that the functions in the frame are not linearly independent (any one of them lies in the closed linear span of all the others). This redundancy is a useful feature in many applications. In other applications, we prefer to reduce the redundancy as much as possible; in the extreme situation the frame becomes linearly independent. A particularly interesting case is presented by orthonormal bases. Standard examples of orthonormal bases are given by

$$g(t) = \begin{cases} 1, & \text{for } 0 \le t \le 1 \\ 0, & \text{otherwise} \end{cases} \tag{8.37}$$

$$t_0 = 1,\ \nu_0 = 1$$

for the windowed Fourier transform, and by the Haar basis,

$$h(t) = \begin{cases} 1, & \text{for } 0 \le t \le 1/2 \\ -1, & \text{for } 1/2 \le t < 1 \\ 0, & \text{otherwise} \end{cases} \tag{8.38}$$

$$a_0 = 2,\ b_0 = 1$$

for the wavelet case. The corresponding g_{mn} and h_{mn} constitute orthonormal bases of $L^2(\mathbb{R})$, with, however, very bad frequency localization, since $G(\omega)$ and $H(\omega)$ decay as $|\omega|^{-1}$ for $|\omega| \to \infty$. This section discusses how this situation can be improved.

8.5.1 Orthonormal Bases and the Windowed Fourier Transform

An orthonormal basis is a frame with frame constants $A = B = 1$. (Conversely, a frame with frame bounds $A = B = 1$, consisting of normalized vectors, $|\phi_j| = 1$ for every $j \in J$,* is necessarily an orthonormal basis.) If the functions

*The index j used here should not be confused with the symbol j for the square root of -1.

$$g_{mn}(t) = e^{2\pi j m v_0 t}\, g(t - v, t_0) \tag{8.39}$$

constitute an orthonormal basis, then by (8.31) this implies $\nu_0 t_0 = 1$. It follows from Theorem 2 that g must necessarily have bad localization in either time or frequency,

$$\int_{-\infty}^{\infty} dt\; t^2 |g(t)|^2 = \infty \quad \text{or} \quad \int_{-\infty}^{\infty} d\omega\; \omega^2 |G(\omega)|^2 = \infty.$$

It is therefore impossible to do much better than (8.37). It turns out we can do slightly better: in [45] an orthonormal basis of type (8.39) is constructed with $\nu_0 = t_0 = 1$ and

$$g(t) = \begin{cases} 0 & t \le -1 \\ \sin \dfrac{(t+1)\pi}{2} & -1 \le t \le 0 \\ \cos^2 \dfrac{(t-n)\pi}{2} \left[-\sin \dfrac{(t-n)\pi}{2} \right]^n & n \le t \le n+1,\ n \in \mathbb{N}. \end{cases}$$

This function is continuous and it is differentiable everywhere except in $t = \pm 1$. Both g and G are absolutely integrable,

$$\int dt\; |g(t)| < \infty, \qquad \int d\omega\; |G(\omega)| < \infty,$$

which is indeed an improvement over (8.37). However, $\int dt\; t^2 |g(t)|^2$ diverges.

It turns out, rather surprisingly, that we can do much better by a slight variant on the construction (8.39). This is outside the scope of the present chapter, so that we will only lightly touch on the subject. If G is well localized, then the G_{mn} as given by (8.39) can be viewed as a "one-bump" function G, translated in frequency, $G_{m0}(\nu) = G(\nu - m\nu_0)$, and multiplied by $e^{2\pi j n t_0 \nu}$ in order to obtain the time localization. Wilson proposed in [46] to generate time-frequency localized functions having two "bumps" in frequency,

$$\Psi_{mn}(t) = \phi_m(t - nt_0), \qquad n \in \mathbb{Z} \tag{8.40}$$

with

$$\hat{\phi}_m(\nu) = f_m^1\ (\nu - m\nu_0) + f_m^2\ (\nu + m\nu_0), \qquad m \in \mathbb{N},$$

where the $f_m^1(\nu), f_m^2(\nu)$ are both peaked around $\nu = 0$. He gave an explicit construction for an orthonormal basis of this type and produced numerical evidence that the f_m^j in his construction have exponential decay in both time and frequency. Wilson's basis has the attractive property that

$$\begin{aligned} &\int dt\; \Psi^*_{mn}(t) \frac{d^2}{dt^2} \Psi_{m'\,n'(t)} \\ &= \int d\nu\; \Psi^*_{mn}(\nu)\, \nu^2\, \Psi_{m'n'}(\nu) = 0 \qquad \begin{array}{l} \text{if } |m - m'| > 1 \\ \text{or if } |m - m'| = 1, |n - n'| > 1. \end{array} \end{aligned} \tag{8.41}$$

In [47] a proof of the exponential decay of Wilson's basis is sketched. If we are willing to give up (8.41), then much simpler "two-frequency-bump" bases of type (8.40) can be constructed, as shown in [48]. The Wilson basis in [48] has "bumps" that all have the same shape; that is,

$$|f_m^1(\nu)| = |f_m^2(\nu)| = f(\nu)$$

is *independent of m*. The function f is proved to have exponential decay in time and in frequency, and can be obtained as a superposition of Gaussians.

8.5.2 Orthonormal Wavelet Bases

The situation is very different in the wavelet case: much nicer bases than the Haar basis exist. The first constructions are due to Stromberg [9], to Meyer [10], and to Battle [13] and Lemarié [12]. In the Meyer basis the function h has a compactly supported, infinitely (many times) differentiable Fourier transform H. It follows that h itself is infinitely (many times) differentiable, and that it decays faster than any inverse polynomial: for all N, there exists C_N so that

$$|h(t)| \leq C_N\,(1 + |t|)^{-N}.$$

For practical purposes, however, the constants C_N turn out to be so large as to give rather bad numerical localization properties. The Stromberg and Battle-Lemarié bases have less differentiability (typically they are k times differentiable), but they have exponential decay in time,

$$|h(t)| \leq C\, e^{-\alpha|t|}.$$

The decay constant α tends to zero as k (the degree of differentiability of h) tends to ∞.

The first constructions of orthonormal bases of wavelets were generally the result of a lot of ad hoc ingenuity, together with seemingly miraculous cancellations. This picture changed with the advent of *multiresolution analysis*, an elegant framework developed by Mallat and Meyer [16], [15], into which all existing nice wavelet bases fit, and that can be used for other wavelet bases constructions. In particular, it can be used to construct orthonormal wavelet bases with compactly supported basic wavelet h [18]. These bases turn out to be related to a special type of quadrature mirror filters. A detailed exposition of many aspects of this construction is given in [18]; a summary of the ideas of multiresolution analysis and a sketch of the construction of [18] will suffice here.

8.5.3 Multiresolution Analysis

The idea of *multiresolution analysis* is to write L^2-functions f as a limit of successive approximations, each of which is a smoothed version of f, with more and more concentrated smoothing functions. The successive approximations thus correspond to different resolutions, whence the name multiresolution analysis. The successive approximation schemes are also required to have some translational invariance. More precisely, a multiresolution analysis consists of

1. A family of embedded closed subspaces $V_m \subset L^2(\mathbb{R})$, $m \in \mathbb{Z}$

$$\cdots \subset V_2 \subset V_1 \subset V_0 \subset V_{-1} \subset V_{-2} \subset \cdots \tag{8.42}$$

such that

2. $$\bigcap_{m \in \mathbb{Z}} V_m = \{0\}, \quad \overline{\bigcup_{m \in \mathbb{Z}} V_m} = L^2(\mathbb{R}) \tag{8.43}$$

and

3. $$f \in V_m \Leftrightarrow f(2\,\cdot) \in V_{m-1} \tag{8.44}$$

Moreover there exists $\phi \in V_0$ such that for all $m \in \mathbb{Z}$, the ϕ_{mn} constitute a *Riesz basis* for V_m, that is,

4. $$\overline{V_m = \text{linear span}\,\{\phi_{mn}, n \in \mathbb{Z}\}} \tag{8.45a}$$

and there exist $0 < A \le B < \infty$ such that, for all $(c_n)_{n\in\mathbb{Z}} \in \ell^2(\mathbb{Z})$,

$$A \sum_n |c_n|^2 \le \left\| \sum_n c_n\, \phi_{mn} \right\|^2 \le B \sum_n |c_n|^2, \tag{8.45b}$$

(in fact, a ***Riesz basis*** is a basis which is also a frame. This excludes bases in which the angle between basis vectors can become arbitrarily small.). Here $\phi_{mn}(x) = 2^{-m/2}\,\phi(2^{-m}x - n)$. Let P_m denote the orthogonal projection onto V_m. It is then clear from (8.42), (8.43) that $\lim_{m \to \infty} P_m f = f$, for all $f \in L^2(\mathbb{R})$. The condition (8.44) ensures that the V_m correspond to different scales, while the translational invariance

$$f \in V_m \to f(\cdot - 2^m n) \in V_m, \qquad \text{for all } n \in \mathbb{Z}$$

is a consequence of (8.45).

Example 8.1

A typical though crude example is the following. Take the V_m to be spaces of piecewise constant functions,

$$V_m = \{f \in L^2(\mathbb{R}); f \text{ constant on } [2^m n, 2^m(n+1)[, \text{ for all } n \in \mathbb{Z}\}.$$

The conditions (8.42)–(8.44) are clearly satisfied. The projections P_m are defined by

$$P_m f\big|_{[2^m n, 2^m(n+1)[} = 2^{-m} \int_{2^m n}^{2^m(n+1)} dx\, f(x).$$

The successive $P_m f$ (as m decreases) do therefore correspond to approximations of f on a finer and finer scale. Finally, we can choose for ϕ the characteristic function of the interval $[0, 1[$,

$$\phi(x) = \begin{cases} 1, & 0 \le x < 1 \\ 0, & \text{otherwise.} \end{cases}$$

Clearly, $\phi \in V_0$, and $V_m = \overline{\text{Span}\ \{\phi_{mn}\}}$.

In what follows, we shall revisit this example to illustrate the construction of an orthonormal wavelet basis from multiresolution analysis.

Note that, in view of (8.44), the condition (8.45) may be replaced by the weaker condition $V_0 = \overline{\text{Span}\ \{\phi_{0n}\}}$. Moreover, we may, without loss of generality, assume that the ϕ_{0n} are orthonormal (which automatically implies that the ϕ_{mn} are orthonormal for every fixed m). If the ϕ_{0n} are not orthonormal to start with, we may then define $\tilde{\phi}$ as the inverse Fourier transform of the following frequency function:

$$\tilde{\Phi}(\xi) = C\ \Phi(\xi) \left(\sum_{k \in \mathbb{Z}} |\Phi\ (\xi + 2k\pi|^2 \right)^{-1/2} \tag{8.46}$$

where we implicitly assume that Φ, the Fourier transform of ϕ, has sufficient decay to make the infinite sum converge. We find that

$$\overline{\text{Span}\ \{\phi_{0n}\}} = \overline{\text{Span}\ \{\tilde{\phi}_{0n}\}},$$

while, moreover, the $\tilde{\phi}_{0n}$ are orthonormal. See [15] for a detailed proof.

Example 8.1 (continued)

In this case the ϕ_{0n} are orthonormal from the start. If we define

$$c_{mn}(f) = \langle \phi_{mn}, f \rangle = 2^{-m/2} \int_{2^m n}^{2^m(n+1)} dx f(x), \tag{8.47}$$

then

$$P_m f = \sum_n c_{mn}(f)\ \phi_{mn}.$$

Let us look at the difference between $P_m f$ and the next coarser approximation $P_{m+1} f$. We may easily check that

$$\phi_{m+1\ n} = \frac{1}{\sqrt{2}} (\phi_{m\ 2n} + \phi_{m\ 2n+1}).$$

Hence

$$c_{m+1\ n}(f) = \frac{1}{\sqrt{2}} [c_{m\ 2n}(f) + c_{m\ 2n+1}(f)].$$

This again exhibits $P_{m+1}f$ as an averaged version of $P_m f$, that is, as a larger-scale approximation. The difference between these two successive approximations is given by

$$P_m f - P_{m+1} f = \frac{1}{2} \sum_n [c_{m\,2n}(f) - c_{m\,2n+1}(f)]\,[\phi_{m\,2n} - \phi_{m\,2n+1}].$$

The remarkable fact about this expression is that it can be rewritten under a form very similar to (8.47). Define

$$\psi(x) = \phi(2x) - \phi(2x-1) = \begin{cases} 1, & 0 \le x < 1/2 \\ -1, & 1/2 \le x < 1 \\ 0, & \text{otherwise} \end{cases} \tag{8.48}$$

Then

$$\begin{aligned} \psi_{mn}(x) &= 2^{-m/2}\,\psi(2^{-m}x - n) \\ &= \frac{1}{\sqrt{2}}(\phi_{m-1\,2n} - \phi_{m-1\,2n+1}), \end{aligned} \tag{8.49}$$

and

$$\begin{aligned} Q_{m+1} f &= P_m f - P_{m+1} f \\ &= \sum_n d_{m+1\,n}(f)\,\psi_{m+1\,n} \end{aligned} \tag{8.50}$$

where

$$d_{m+1\,n}(f) = \langle \psi_{m+1\,n}, f \rangle = \frac{1}{\sqrt{2}}[c_{m\,2n}(f) - c_{m\,2n+1}(f)].$$

What is so remarkable about this? Note first, as can easily be checked from (8.48), that for fixed m the ψ_{mn} are orthonormal. The decomposition (8.50) is thus the expansion, with respect to an orthonormal basis, of $Q_{m+1}f$, the orthogonal projection of f onto $W_{m+1} = P_m L^2 - P_{m+1}L^2$, that is, onto the orthogonal complement of V_{m+1} in V_m. The surprising fact is that, as is clear from (8.50), the W_m are also (as are the V_m) generated by the translates and dilates ψ_{mn} of a single function ψ. Once this is realized, building a wavelet basis becomes trivial. Clearly (8.42)–(8.43), together with $W_m \perp V_m$, $V_{m-1} = V_m \oplus W_m$, imply that the W_m are all mutually orthogonal and that their direct sum is $L^2(\mathbb{R})$. Since for each m, the set $\{\psi_{mn};\, n \in \mathbb{Z}\}$ constitutes an orthonormal basis for W_m, it follows that the whole collection $\{\psi_{mn};\, m, n \in \mathbb{Z}\}$ is an orthonormal wavelet basis for $L^2(\mathbb{R})$.

In the example above, the function ψ is nothing but the Haar function (see (8.38)), and it is therefore no surprise that the ψ_{mn} constitute an orthonormal basis. The example does, however, clearly show how this basis can be constructed from a multiresolution analysis. Let us sketch now how the general case works.

For a multiresolution analysis, that is, a family of spaces V_m and a function ϕ satisfying (8.42)–(8.44), we may define (as in example 8.1) W_m as the orthogonal complement, in V_{m-1}, of V_m,

$$V_{m-1} = V_m \oplus W_m, \qquad W_m \perp V_m. \tag{8.51}$$

Equivalently,

$$W_m = Q_m L^2(\mathbb{R}), \qquad \text{with } Q_m = P_{m-1} - P_m. \tag{8.52}$$

It follows immediately that all the W_m are scaled versions of W_0,

$$f \in W_m \Leftrightarrow f(2^m \cdot) \in W_0, \tag{8.53}$$

and that the W_m are orthogonal spaces which sum to $L^2(\mathbb{R})$,

$$L^2(\mathbb{R}) = \bigoplus_{m \in \mathbb{Z}} W_m. \tag{8.54}$$

Because of the properties (8.42)–(8.45) of the V_m, it turns out [14], [15] that in W_0 also (as in V_0) there exists a vector ψ such that its integer translates span W_0, that is,

$$\overline{\text{Span}\ \{\psi_{0n}\}} = W_0, \tag{8.55}$$

where $\bar{A}$ denotes the closure of A, that is, the set of all the functions in $L^2(\mathbb{R})$ that can be approximated with arbitrary precision by elements of A. As before, $\psi_{mn}(x)$ stands for $2^{-m/2}\,\psi(2^{-m}x - n)$, for $m,n \in \mathbb{Z}$. It follows immediately from (8.53) that then

$$\overline{\text{Span}\ \{\psi_{mn}\}} = W_m,$$

for all $m \in \mathbb{Z}$.

Intuitively we may understand this similarity between W_0 and V_0 by the fact that V_{-1} is "twice as large" as V_0, since V_0 is generated by the integer translates of a single function $\phi_{0\,0}$, while V_{-1} is generated by the integer translates of *two* functions, namely, $\phi_{-1\,0}$ and $\phi_{-1\,1}$. It therefore seems natural that the orthogonal complement W_0 of V_0 in V_{-1} is also generated by the integer translates of a single function. This hand-waving argument can easily be made rigorous by using group representation arguments. A mere proof of *existence* of a function ψ satisfying (8.55) would, however, not be enough for practical purposes. A more detailed analysis leads to the following algorithm for the *construction* of ψ [14], [15]. We start from a function ϕ such that the ϕ_{0n} are an orthonormal basis for V_0 (if necessary, we apply (8.46)). Since

$$\phi \in V_0 \subset V_{-1} = \overline{\text{Span}\ \{\phi(2\cdot - n)\}},$$

there exist c_n such that

$$\phi(x) = \sum_n c_n\, \phi(2x - n). \tag{8.56}$$

Define then

$$\psi(x) = \sum_n (-1)^n \, c_{n+1} \, \phi(2x + n) \tag{8.57}$$

The corresponding ψ_{0n} will constitute an orthonormal basis of W_0 [14], [15]. Consequently, the ψ_{mn}, for fixed m, will constitute an orthonormal basis of W_m. It follows then from (8.53) that the $\{\psi_{mn},\ m, n \in \mathbb{Z}\}$ constitute an orthonormal basis of wavelets for $L^2(\mathbb{R})$. This completes the explicit construction, in the general case, of an orthonormal wavelet basis from a multiresolution analysis.

Example 8.1 (final visit)

As we already noted, the ϕ_{0n} are orthonormal in this example, and

$$\phi(x) = \phi(2x) + \phi(2x - 1).$$

Applying the recipe (8.56)–(8.57) then leads to

$$\psi(x) = \phi(2x) - \phi(2x - 1),$$

which corresponds to (8.48).

Remarks

1. We can show [15] that the functions ϕ, ψ having all the above properties necessarily satisfy

$$\int dx\ \psi(x) = 0 \tag{8.58}$$

and

$$\int dx\ \phi(x) \neq 0, \tag{8.59}$$

where we implicitly assume that ϕ, ψ are sufficiently well behaved for these integrals to make sense (in all examples of practical interest, $\phi, \psi \in L^1$). In fact we do not even need to assume that the ϕ_{0n} or ψ_{0n} are orthonormal to derive (8.58)–(8.59). We saw in Section 8.4 that (8.58) has to be satisfied even if the ψ_{mn} constitute only a frame. Note also that the transition (8.46) from ϕ to $\tilde{\phi}$, orthonormalizing the ϕ_{0n}, preserves $\int dx\ \phi(x) \neq 0$.

2. If we restrict ourselves to the case where ϕ is a *real* function (as in all the examples above), then ϕ is determined uniquely, up to a sign, by the requirement that the ϕ_{0n} be orthonormal. We then also have $\int dx\ \phi(x) = \pm 1$; we shall fix the sign of ϕ so that

$$\int dx\ \phi(x) = 1.$$

In practice we can often start the whole construction by choosing an appropriate ϕ, that is, a function ϕ satisfying (8.56) for some c_n. Provided ϕ is "reasonable" (it suffices, for example, that $\inf_{|\xi| \geq \pi} |\Phi(\xi)| > 0$ and that $\sum_{k \in \mathbb{Z}} |\Phi(\xi + 2\pi k)|^2$ is bounded), the closed linear spans V_m of the ϕ_{mn} (m fixed) then automatically satisfy (8.42)–(8.45). There exists then an associated orthonormal basis of wavelets. Two typical examples are as follows:

Example 8.2

$$\phi(x) = \begin{cases} x. & 0 \leq x \leq 1 \\ 2 - x, & 1 \leq x \leq 2 \\ 0, & \text{otherwise.} \end{cases}$$

This is the linear B-spline function; the spaces V_m consist of continuous, piecewise linear functions. The c_n are given by

$$\phi(x) = \frac{1}{2}\phi(2x) + \phi(2x - 1) + \frac{1}{2}\phi(2x - 2).$$

Example 8.3

$$\phi(x) = \begin{cases} x^2, & 0 \leq x \leq 1 \\ -2x^2 + 6x - 3, & 1 \leq x \leq 2 \\ (3 - x)^2, & 2 \leq x \leq 3 \\ 0, & \text{otherwise.} \end{cases}$$

This is the quadratic B-spline function; the spaces V_m consist of C^1, piecewise quadratic functions. The c_n are given by

$$\phi(x) = \frac{1}{4}\phi(2x) + \frac{3}{4}\phi(2x - 1) + \frac{3}{4}\phi(2x - 2) + \frac{1}{4}\phi(2x - 3).$$

In these last two examples the corresponding ψ will be respectively continuous and piecewise linear, or C^1 and piecewise quadratic. Starting from spline functions we can, in fact, construct orthonormal bases of wavelets with an arbitrarily high number of continuous derivatives. These bases are the Battle-Lemarié bases [13], [12], [15]. In these constructions the initial function ϕ is compactly supported, but the ϕ_{0n} are not orthogonal, as illustrated by the two examples. We therefore have to apply (8.46) before using (8.56), (8.57); the transition $\phi \rightarrow \tilde{\phi}$ in (8.46) leads to a noncompactly supported $\tilde{\phi}$, resulting in a noncompactly supported ψ. Typically, the Battle-Lemarié wavelets have exponential decay.

Up to now, we have restricted ourselves to one dimension. It is very easy, however, to extend the multiresolution analysis to more dimensions. This extension was already inherent in the first construction by Lemarié and Meyer [11] of an n-dimensional wavelet basis. It becomes much more transparent, however, from the multiresolution analysis point of view. Let us illustrate this for two dimensions. The case of n dimensions, n arbitrary, is completely similar. Assume that we dispose of a one-dimensional multiresolution analysis, that is, we have at hand a ladder of spaces V_m, and functions ϕ, ψ satisfying (8.42)–(8.45) and (8.55), where the ϕ_{0n} and the ψ_{0n} are assumed to be orthonormal. Define then

$$\mathbf{V}_m = V_m^1 \otimes V_m^2.$$

where we use the notation $A^1 \otimes B^2$ for the space spanned by all the functions of the type $f(x_1, x_2) = a(x_1)\, b(x_2)$, with $a \in A$, $b \in B$. Clearly the $\mathbf{V}_m$ define a ladder of subspaces of $L^2(\mathbb{R}^2)$, satisfying (8.42) and the equivalent, for $\mathbb{R}^2$, of (8.43). Moreover (8.44) holds, and if we define

$$\Phi(x_1, x_2) = \phi(x_1)\phi(x_2),$$

then this two-dimensional function satisfies the analog of (8.45),

$$\mathbf{V}_m = \overline{\text{Linear span }\{\Phi_{mn};\, n \in \mathbb{Z}^2\}},$$

where Φ_{mn} is defined by

$$\begin{aligned}\Phi_{mn}(x_1, x_2) &= 2^{-m}\Phi(2^{-m}x_1 - n_1, 2^{-m}x_2 - n_2)\\ &= \phi_{mn1}(x_1)\, \phi_{mn2}(x_2).\end{aligned}$$

Note that we use the *same* dilation for both arguments. Because of the definition (8.51) of W_m, we find immediately that

$$\mathbf{V}_{m-1} = \mathbf{V}_m \oplus [(V_m^1 \otimes W_m^2) \oplus (W_m^1 \otimes V_m^2) \oplus (W_m^1 \otimes W_m^2)].$$

This implies that an orthonormal basis for the orthogonal complement $\mathbf{W}_m$ of $\mathbf{V}_m$ in $\mathbf{V}_{m-1}$ is given by the functions $\phi_{mn_1}\psi_{mn_2}$, $\psi_{mn_1}\, \phi_{mn_2}$, $\psi_{mn_1}\, \psi_{mn_1}$, with $n_1, n_2 \in \mathbb{Z}$ or equivalently, by the two-dimensional wavelets Ψ^ℓ_{mn},

$$\Psi^\ell_{mn}(x_1, x_2) = 2^{-m}\Psi^\ell(2^{-m}x_1 - n_1, 2^{-m}x_2 - n_2), \tag{8.60}$$

where $\ell = 1, 2, 3$, and $n \in \mathbb{Z}^2$ and with

$$\Psi^1(x_1, x_2) = \phi(x_1)\, \psi(x_2) \tag{8.61}$$

$$\begin{aligned}\Psi^2(x_1, x_2) &= \psi(x_1)\phi(x_2)\\ \Psi^3(x_1, x_2) &= \psi(x_1)\psi(x_2).\end{aligned} \tag{8.62}$$

It follows that the Ψ^ℓ_{mn}, $\ell = 1, 2, 3$, $m \in \mathbb{Z}$, and $n \in \mathbb{Z}^2$, constitute an orthonormal basis of wavelets for $L^2(\mathbb{R}^2)$.

The above construction shows how any multiresolution analysis plus associated wavelet basis in one dimension can be extended to d dimensions. The decomposition plus reconstruction algorithm constructed by Mallat for visual data [16] uses such a two-dimensional basis.

8.5.4 The Connection with Discrete Filters

Multiresolution analysis can be used to decompose discrete sequences of data (corresponding to time series, or, in two dimensions, to television images) into several "layers" corresponding to the content of the original sequence in different frequency bands, with each component sequence sampled at a lower rate, adapted to its frequency content. This scheme was first proposed by Mallat [16]. Let us show explicitly how his algorithm works.

We associate a function $f \in V_0$ with the original sequence $(c_n)_{n \in \mathbb{Z}}$ by defining

$$f = \sum_{n \in \mathbb{Z}} c_n^0 \phi_{0n}$$

(we have attached a superscript 0 to the data sequence). Since $V_0 = V_1 \oplus W_1$, f can be decomposed uniquely into an element of V_1 plus an element of W_1; these two components can be expanded into the ϕ_{1n} and ψ_{1n}, respectively (since $(\phi_{1n})_{n \in \mathbb{Z}}$ is an orthonormal basis of V_1, and $(\psi_{1n})_{n \in \mathbb{Z}}$ an orthonormal basis of W_1),

$$\begin{aligned} f &= P_1 f + Q_1 f \\ &= \sum_{n \in \mathbb{Z}} c_n^1 \phi_{1n} + \sum_{n \in \mathbb{Z}} d_n^1 \psi_{1n}. \end{aligned}$$

The sequences c_n^1, d_n^1 can be computed directly from the c_n^0:

$$\begin{aligned} c_n^1 &= \langle \phi_{1n}, P_1 f \rangle = \langle \phi_{1n}, f \rangle \\ &= \sum_k c_k^0 \langle \phi_{1n}, \phi_{0k} \rangle \\ &= \sum_k c_k^0 \, h_{2n-k} \end{aligned} \tag{8.63}$$

with

$$h_k = \frac{1}{\sqrt{2}} \int dx \, \phi(x/2) \, \phi(x+k). \tag{8.64}$$

Similarly

$$d_n^1 = \sum_k c_k^0 \, g_{2n-k}, \tag{8.65}$$

with

$$g_k = \frac{1}{\sqrt{2}} \int dx \, \psi(x/2) \, \phi(x+k). \tag{8.66}$$

Since $\int dx\, \phi(x) = 1$ (see Section 8.5.3), the sequence c_n^1 can be considered as an "averaged" version of the c_k^0, on a scale twice as large, and therefore sampled only half as often, as expressed by (8.63), which is a convolution followed by a "decimation" with factor 2. The sequence d_n^1 corresponds to the difference in information between the original c_n^0 and the averaged version c_n^1; the d_n^1 also "live" on a scale twice as large as the c_n^0, as shown by (8.65). The original sequence c_n^0 can be reconstituted from the c_n^1 and d_n^1, using the *same* coefficients h_k and g_k:

$$\begin{aligned} c_n^0 &= \langle \phi_{0n}, f \rangle = \langle \phi_{0n}, P_1 f + Q_1 f \rangle \\ &= \sum_k c_k^1 \langle \phi_{0n}, \phi_{1k} \rangle + \sum_k d_k^1 \langle \phi_{0n}, \Psi_{1k} \rangle \\ &= \sum_k \left[c_k^1 h_{2k-n} + d_k^1 g_{2k-n} \right]. \end{aligned} \tag{8.67}$$

The decomposition of c_n^0 into c_n^1 and d_n^1 is only the first stage of the game. In the next stage, we decompose c_n^1 into an even coarser average sequence c_n^2 and a new "difference" sequence d_n^2. To do this, we again use multiresolution analysis as a tool:

$$\begin{aligned} P_1 f \in V_1 &= V_2 \oplus W_2 \\ \Longrightarrow \quad P_1 f &= P_2 f + Q_2 f \\ &= \sum_n c_n^2 \phi_{2n} + \sum_n d_n^2 \phi_{2n} \end{aligned}$$

with

$$\begin{aligned} c_n^2 &= \langle \phi_{2n}, P_2 f \rangle = \langle \phi_{2n}, P_1 f \rangle \\ &= \sum_n c_k^1 \langle \phi_{2n}, \phi_{1k} \rangle. \end{aligned}$$

We may easily check that $\langle \phi_{2n}, \phi_{1k} \rangle = \langle \phi_{1n}, \phi_{0k} \rangle = h_{2n-k}$; hence

$$c_n^2 = \sum_n c_k^1 h_{2n-k}. \tag{8.68}$$

Similarly

$$d_n^2 = \sum_n c_k^1 g_{2n-k}. \tag{8.69}$$

We also find, analogously to (8.67), that

$$c_n^1 = \sum_k \left[c_k^2 h_{2k-n} + d_k^2 g_{2k-n} \right]. \tag{8.70}$$

It is now clear how to construct a tree algorithm for the decomposition of the c_n^0 into the different resolution "layers", by iterating the same procedure. If we define the maps H and G from the sequence of square summable sequences $\ell^2(\mathbb{Z})$ to itself by

$$(H\,a)_n = \sum_k h_{2n-k} a_k$$

$$(G\,a)_n = \sum_k g_{2n-k} a_k,$$

with adjoint maps

$$(H^* a)_k = \sum_n h_{2n-k} a_n$$

$$(G^* a)_k = \sum_n g_{2n-k} a_n,$$

then the whole decomposition plus reconstruction scheme can be represented as in Fig. 8.8. For any L, c^0 is decomposable into $d^1, \ldots, d^L$ and c^L.

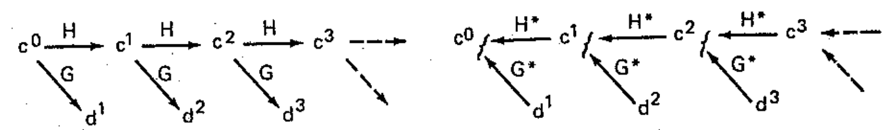

Figure 8.8 Schematic representation of the tree algorithm for the decomposition and reconstruction in Mallat's scheme.

The tree structure, together with the easy convolution and decimation structure of H, G, makes this algorithm work very fast; the whole decomposition can be done faster than an FFT. Note that at every level c^ℓ is replaced by a roughly equivalent number of entries: if the c_n^ℓ are zero except for N consecutive entries, then, apart from edge effects, only $N/2$ entries of $c^{\ell+1}$, $d^{\ell+1}$ will be nonvanishing. The total number of relevant entries in $d^1, d^2, \ldots, d^L, c^L$ is therefore essentially the same as in the original sequence c^0.

In fact, for the implementation of Mallat's algorithm, we only need the two filters G, H; their multiresolution analysis origins are not used explicitly. We may therefore try to isolate the relevant properties of the filters and design filters satisfying all these properties directly, without multiresolution analysis. From (8.63), (8.65), and (8.67) a first condition (C1) can be derived.

Condition 1:

$$H^* H + G^* G = Id.$$

A second condition (C2) expresses the fact that H is an "averaging operator," that is, a low-pass filter, while G measures the difference between a sequence and its average, and is therefore a band pass filter. This results in

Condition 2:

$$\sum_n g(n) = 0$$

$$\sum_n h(n) = \sqrt{2}$$

where the $\sqrt{2}$-normalization is due to the decimation 2:1 in the definition of the filter H (see [18]). Finally, we also impose a regularity condition. The complete reconstruction formula for c^0 from $d^1, d^2, \ldots, d^L, c^L$ is

$$c^0 = G^*d^1 + H^*G^*d^2 + \cdots + (H^*)^{L-1}G^*d^L + (H^*)^L c^L.$$

When iterated many times, the operator H^* should therefore not lead to something too hectic. One way of visualizing this is to represent any sequence by a piecewise constant function, with the heights of the different levels given by the coefficients. The "elementary" sequence $e_n = 1$ for $n = 0$, $e_n = 0$ for $n \neq 0$ is then represented by the function

$$(f_e)(x) = \begin{cases} 1, & -1/2 < x < 1/2 \\ 0, & \text{otherwise.} \end{cases}$$

Our regularity condition (C3) then reads as:

Condition 3: The piecewise constant functions representing $(H^*)^\ell e$ (where $e_n = 0$ for $n \neq 0$, $e_0 = 1$) converge to a "nice" function as $\ell \to \infty$.

For a more precise formulation of this condition, see [18]. Filters H, G, which are derived from a multiresolution analysis, automatically satisfy conditions (C1)–(C2). Moreover, we can show that in this case the piecewise constant functions representing $(H^*)^\ell e$ converge to the averaging function ϕ itself [18], so that (C3) is also satisfied. It is possible to construct filters H, G which satisfy (C1)–(C2), but not (C3). An example is given in Fig. 8.9. In this case the $(H^*)^\ell e$ converge, for $\ell \to \infty$, to a distribution which is singular at every dyadic rational between 0 and 3, that is, every point of the form $k2^{-m}$, with $0 \leq k < 3\ 2^m$. This example shows that condition (C3) is necessary to avoid "messy" iterations.

It turns out [18] that conditions (C1)–(C3) ensure that the filters H, G are associated to a multiresolution analysis. The "averaging function" ϕ of that multiresolution analysis is exactly the "nice" function to which the $(H^*)^\ell e$-piecewise constant functions converge. The proof in [18] of this equivalence between filters and

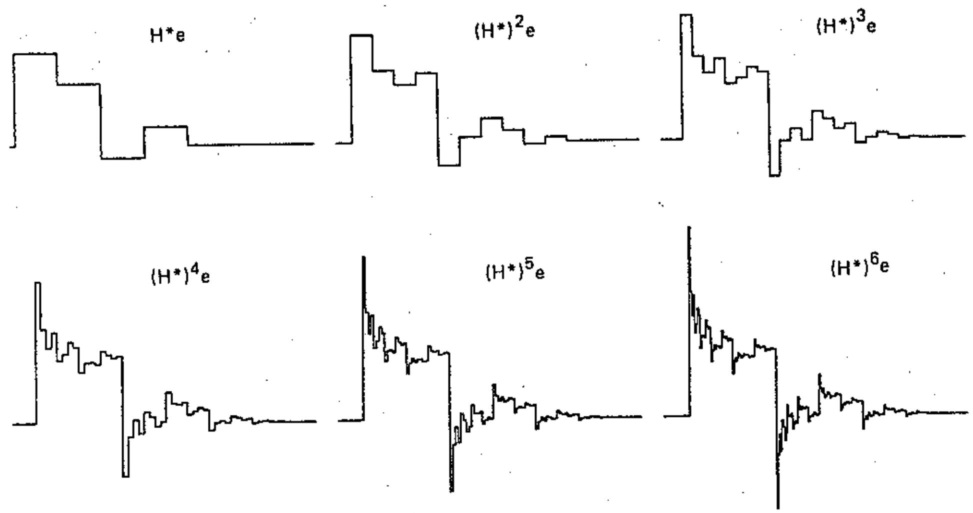

Figure 8.9 A pair of filters H, G that do satisfy (C1)–(C2), but not (C3). In this case $h_0 = 15\,\alpha$, $h_1 = 10\,\alpha$, $h_2 = -2\,\alpha$, $h_3 = 3\,\alpha$, with $\alpha = (13\sqrt{2})^{-1}$, and all other $h_k = 0$. The g_k are defined by $g_k = (-1)^k\,h(-k+1)$.

orthonormal bases of wavelets essentially uses this "graphical" construction of ϕ as a limit of piecewise constant functions representing sequences.

The filters H, G are special cases of *quadrature mirror filters,* developed by Esteban and Galand [49] for subband coding with reconstruction without aliasing. The multiresolution filters H and G give exact reconstruction: not only is there no aliasing, but amplitude and phase distortion are absent as well. Quadrature mirror filters leading to exact reconstruction were first developed by Smith and Barnwell [50], who called them *conjugate quadrature filters.* General quadrature filters do not satisfy our regularity condition, however.

8.5.5 Orthonormal Bases of Compactly Supported Wavelets

The equivalence between filters H, G satisfying conditions (C1)–(C3) and multiresolution analysis can be exploited to construct orthonormal bases different from the examples shown so far. We may easily check that the graphical representation of $(H^*)^\ell e$, as a piecewise constant function with stepwidth $2^{-\ell}$, is supported on $[-2^{-\ell-1}, K(1-2^{-\ell}) + 2^{-\ell-1}]$ if the filter H has a finite number of taps: $h_k = 0$ for $k < 0$ or $k > K$. It follows that the limit function, which is nothing but the averaging function ϕ of the multiresolution analysis, is supported on $[0, K]$. As a finite linear combination of translates and dilates of ϕ, the wavelet ψ therefore also has compact support; one finds support $\psi \subset [-(K-1)/2, (K+1)/2]$ (see [18]). It therefore suffices to find finite filters H, G satisfying the conditions (C1)–(C3) in order to have an orthonormal basis of compactly supported wavelets. In [18] this method is used to build an infinite family of functions ${}_N\psi$. For each $N \in \mathbb{N}$, these ${}_N\psi$ have the following properties:

- support ${}_N\psi = [-(N-1), N]$ (8.71)
- ${}_N\psi_{mn}(t) = 2^{-m/2}({}_N\psi)(2^{-m}t - n)$ (8.72)

  constitute an orthonormal basis of $L^2(\mathbb{R})$

- $$\int_{-\infty}^{\infty} dt\, t^k\, {}_N\psi_{mn}(t) = 0, \qquad k = 0, 1, \ldots, N-1 \tag{8.73}$$

- $$|({}_N\psi)^\wedge(\nu)| \le C_N(1 + |\nu|)^{-0.1936\, N} \tag{8.74}$$

For $N = 1$, ${}_1\psi$ is the Haar function. As N increases, the functions ${}_N\psi$ become more regular, as shown by the decay of their Fourier transform (8.74), and have more moments equal to zero, as shown by (8.73). The price to pay for these desirable features is that the support of ${}_N\psi$ increases (see (8.71)). Figure 8.10 shows the functions ${}_N\psi$ and the corresponding averaging function ${}_N\phi$ for $N = 2, 6, 10$.

A very recent application of orthonormal bases of wavelets is in numerical analysis. Beylkin, Coifman, and Rokhlin [51] have developed an algorithm that uses multiresolution analysis for large matrix computations, for example. They claim that even for matrices of "convolutional" character, that is, $M_{ij} = m(i-j)$, their algorithm beats FFT by a wide margin if the matrices are very large (more than $(2^{10})^2$ entries). They use in particular the compactly supported orthonormal bases presented here, because the corresponding filters have finitely many taps, and because of the "vanishing moments" property (8.73).

8.6 CONCLUSION

In this chapter we have presented different aspects of the wavelet transform, a linear transform that can be used as a tool for time-frequency analysis. It has the attractive feature that high-frequency wavelets have a much smaller support in time than low-frequency wavelets, which makes the wavelet transform particularly well suited for the analysis of signals with high-frequency transients superposed on longer-lived low-frequency components. We have reviewed three different forms of the wavelet transform: the continuous wavelet transform, frames of wavelets, and orthonormal wavelet bases. In the first two cases, the formulation is analogous to the windowed Fourier transform, which we have discussed in parallel with the wavelet transform. The main difference is that the wavelet transform handles frequency logarithmically rather than linearly, resulting in an analysis with constant $\Delta\nu/\nu$. The third form of the wavelet transform uses orthonormal bases of wavelets with good localization in both

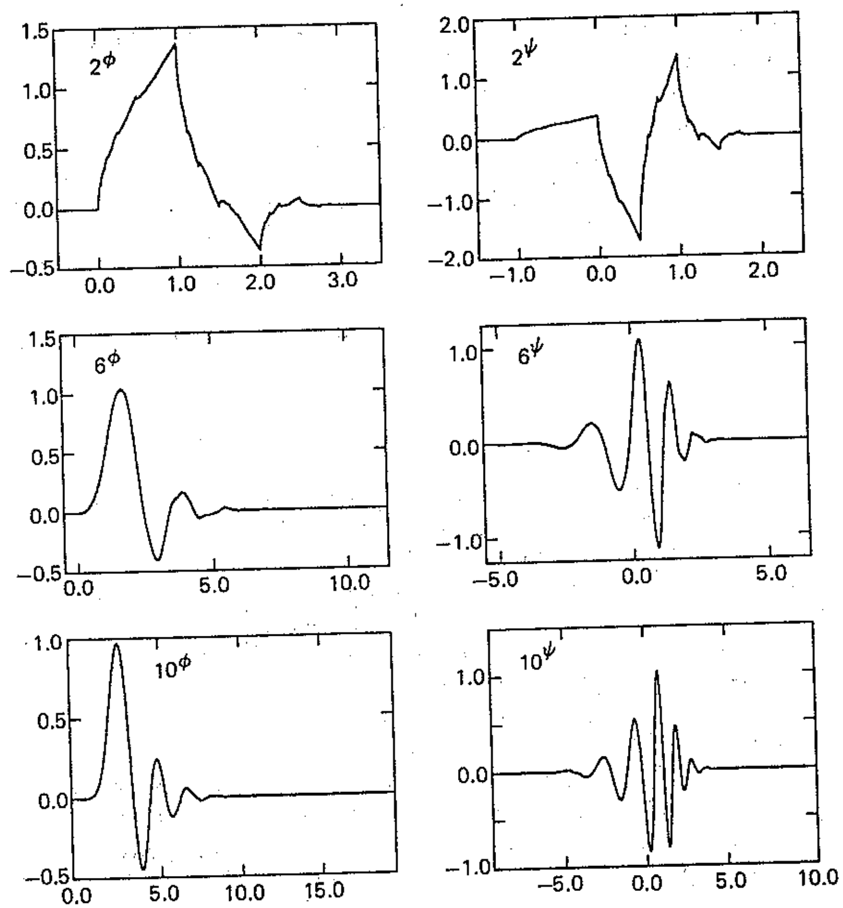

Figure 8.10 The wavelets $_N\psi$ and the corresponding averaging functions $_N\phi$ for $N = 2, 6, 10$.

time and frequency; these have no analog in the windowed Fourier case. We have reviewed their construction and given a few examples. Orthonormal bases of wavelets turn out to be related to special filters for subband coding that lead to exact reconstruction, without aliasing and without amplitude or phase distortion. The wavelet transform is fairly new, even though it is related to techniques in signal analysis that are well established (constant $\Delta\nu/\nu$ filtering, subband coding). The mathematical theory presented here gives a new way of looking at these standard techniques, which may lead to new applications. Examples are the finitely supported wavelet bases of Section 8.5.5; they are functions corresponding to special quadrature mirror filters with an extra regularity condition. To my knowledge, noboby had represented QMF filters by these functions before; indeed, without the regularity condition such a representation would be meaningless. This representation has led to a new application of QMF filters to numerical analysis. Other fields where the wavelet transform is currently applied are acoustics and image analysis.

REFERENCES

1. J. Morlet, "Sampling Theory and Wave Propagation," in pp. 233–261 of *NATO ASI Series*, Vol. 1, *Issues in Acoustic Signal/Image Processing and Recognition*, C. H. Chen, ed. (Berlin: Springer 1983).
2. J. Morlet, G. Arens, I. Fourgeau, and D. Giard, "Wave Propagation and Sampling Theory," *Geophysics* 47 (1982), 203–236.
3. A Grossmann and J. Morlet, "Decomposition of Hardy Functions into Square Integrable Wavelets of Constant Shape," *SIAM J. Math. Anal.* **15** (1984), 723–736.
4. A. Grossmann and J. Morlet, "Decomposition of Functions into Wavelets of Constant Shape, and Related Transforms," in *Mathematics and Physics*, Lectures on recent results (Singapore: World Scientific, 1985).
5. P. Goupillaud, A. Grossmann, and J. Morlet, "Cycle-Octave and Related Transforms in Seismic Signal Analysis," *Geoexploration* **23** (1984), 85.
6. A Grossmann, J. Morlet, and T. Paul, "Transforms Associated to Square Integrable Group representations, I," *J. Math. Phys.* **26** (1985), 2473–2479; "II," *Ann. Inst. Henri Poincaré* **45** (1986), 293–309.
7. I. Daubechies, A. Grossmann, and Y. Meyer, "Painless Non-orthogonal Expansions," *J. Math. Phys.* **27** (1986), 1271–1283.
8. I. Daubechies, "The Wavelet Transform, Time-Frequency Localization and Signal Analysis," *IEEE Trans. Information Theory*, September 1990.
9. J. O. Stromberg, "A Modified Franklin System and Higher Order Spline Systems on $\mathbb{R}^n$ as Unconditional Bases for Hardy Spaces," in pp. 475–493 of *Conf. in Honor of A. Zygmund*, Vol. II, W. Beckner et al. eds. (Belmont, Calif.: Wadsworth, 1981).
10. Y. Meyer, "Principe d'incertitude, bases hilbertiennes et algèbres d'opérateurs," *Séminaire Bourbaki*, 1985–1986, nr. 662.
11. P. G. Lemarié and Y. Meyer, "Ondelettes et bases hilbertiennes," *Rev. Math. Iberoamericana* **2** (1986), 1–18.
12. P. G. Lemarié, "Une nouvelle base d'ondelettes de $L^2(\mathbb{R}^n)$," *J. de Math. Pures et Appl.* **67** (1988) 227-236.
13. G. Battle, "A Block Spin Construction of Ondelettes. Part I: Lemarié Functions," *Comm. Math. Phys.* **110** (1987), 601–615.
14. S. Mallat, "Multiresolution Approximation and Wavelets," preprint GRASP Lab, Dept. of Computer and Information Science, Univ. of Pennsylvania (1987); *Trans. Am. Math. Soc.* **315** (1989) 69–88.
15. Y. Meyer, "Ondelettes, function splines, et analyses graduées," Univ. of Torino (1986).
16. S. Mallat, "A Theory for Multiresolution Signal Decomposition: The Wavelet Representation," *IEEE Trans. Pattern Analysis and Machine Intelligence* **11** (1989), 674–693.
17. S. Mallat, "Multifrequency Channel Decompositions of Images and Wavelet Models," *IEEE Proc. Acoustics, Speech, and Signal Processing.* **37** (1989) 2091-2110.
18. I. Daubechies, "Orthonormal Basis of Compactly Supported Wavelets," *Comm. Pure & Applied Math.* **41** (1988), 909–996.
19. R. Kronland-Martinet, J. Morlet, and A. Grossmann, "Analysis of Sound Patterns Through Wavelet Transforms," *Int. J. of Pattern Recognition and Art. Int.* **1** (1987), 273–301.

20. P. Dutilleux, A. Grossmann, and R. Kronland-Martinet, "Application of the Wavelet Tra form to the Analysis, Transformation and Synthesis of Musical Sounds," *Proc. 25th* *Convention,* 1988, nr. 2727 (section A-2).
21. A. Grossmann, "Wavelet Transforms and Edge Detection," in *Stochastic Processes in Ph ics and Engineering,* Ph. Blanchard, L. Streit, and M. Hasewinkel, eds. (Reidel, 1987
22. A. Grossmann, M. Holschneider, R. Kronland-Martinet, and J. Morlet, "Detection of abr changes in sound signals with the help of wavelet transforms," in pp. 289–306 of *Adv. Electronics and Electron Physics,* Suppl. **19**, "Inverse Problems: An Interdisciplin Study," P. C. Sabatier ed. (New York: Academic Press, 1987).
23. F. Argoul, A. Arnéodo, J. Elezgaray, G. Grasseau, and R. Murenzi, "Wavelet Transform Fractal Aggregates," *Phys. Lett. A* **135** (1989), 327.
24. J. R. Klauder and E. Sudarshan, *Fundamentals of Quantum Optics* (New York: Benjan 1968).
25. D. Gabor, "Theory of communication," *J. Inst. Electr. Engin.* (London) **93**: 3 (1946), 42 457.
26. I. Daubechies, "Time-frequency Localization Operators—A Geometric Phase Sp Approach," *IEEE Trans. Information Theory* 34 (1988), 605–612.
27. D. Slepian and H. O. Pollak, "Prolate Spheroidal Wave Functions, Fourier Analysis a Uncertainty, I", *Bell. Syst. Techn. J.* **40** (1961), 43–64.
28. H. J. Landau and H. O. Pollak, "Prolate Spheroidal Wave Functions, Fourier Analysis a Uncertainty, II", *Bell Syst. Techn. J.* **40** (1961), 65–84; H. J. Landau and H. O. Poll "________ III," *Bell Syst. Techn. J.* **41** (1962), 1295–1336.
29. D. Slepian, "On Bandwidth," *Proc. IEEE* 64 (1976), 292–300.
30. D. Thomson, "Spectrum Estimation and Harmonic Analysis," *Proc. IEEE* 70 (1982) 105 1096.
31. A. Grossmann and R. Kronland-Martinet, "Time-and-Scale Representations Obtain Through Continuous Wavelet Transforms," in pp. 475–482 of *Signal Processing IV: Th ories and Applications, Proc. of EUSIPCO-88,* J. L. Lacoume et al., eds. (Amsterda North-Holland, 1988).
32. G. Sarraco, A. Grossmann, and Ph. Tchamitchian, "Use of Wavelet Transforms in the Stu of Propagation of Transient Acoustic Signals Across a Plane Interface Between Two Hon geneous Media," *Proceedings of the International Workshop,* "Wavelets and Time F quency Methods," Marseille, Dec 14–18, 1987, eds. J. M. Combes, A. Grossmann and I Tchamitchian (Springer, 1989).
33. I. Daubechies and T. Paul, "Time-Frequency Localization Operators—A Geometric Pha Space Approach. II, The Use of Dilations," *Inverse Problems* 4 (1988), 661–680.
34. R. J. Duffin and A. C. Schaeffer, "A Class of Nonharmonic Fourier Series," *Trans. Am. Ma Soc.* 72 (1952), 341–366.
35. R. M. Young, *An Introduction to Nonharmonic Fourier Series* (New York: Acaden Press, 1980).
36. H. Landau, "On the density of phase-space expansions." preprint AT&T Bell Laboratori 1989.
37. R. Balian, "Un principe d'incertitude fort en théorie du signal en mécanique quantique," *R. Acad. Sc. Paris* 292, série 2 (1981).

38. F. Low, "Complete Sets of Wave-packets," in pp. 17–22 of *"A Passion for Physics—Essays in Honor of Geoffrey Chew,* (Singapore: World Scientific, 1985) editors: C. DeTar, J. Finkelstein, C-I Tan.

39. G. Battle, "Heisenberg Proof of the Balian-Low Theorem," *Lett. Math. Phys.* **15** (1988), 175–177.

40. I. Daubechies and A. J. E. M. Janssen, "Two Theorems on Lattice Expansions," submitted to *IEEE Trans. Information Theory.*

41. M. J. Bastiaans, "Gabor's Signal Expansion and Degrees of Freedom of a Signal," *Proc. IEEE* **68** (1980), 538–539. See also M. J. Bastiaans, "A Sampling Theorem for the Complex Spectrogram and Gabor's Expansion of a Signal in Gaussian Elementary Signals," *Optical Engineering* **20** (1981), 594–598.

42. A. J. E. M. Janssen, "Gabor Representation of Generalized Functions," *J. Math. Appl.* **80** (1981), 377–394. See also A. J. E. M. Janssen, "Gabor Representation and Wigner Distribution of Signals," *Proc. IEEE* (1984), 41.B.2.1–41.B.2.4.

43. Ph. Tchamitchian, "Calcul symbolique sur les opérateurs de Caldéron-Zygmund et bases inconditionnelles de $L^2(\mathbb{R}^n)$," *C. R. Acad. Sc. Paris.* **303**, série 1 (1986), 215–218. See also Ph. Tchamitchian, "Biorthogonalité et théorie des opérateurs," *Rev. Math. Iberoamericana.,* **3** (1987), nr. 2

44. M. Holschneider, R. Kronland-Martinet, J. Morlet, and Ph. Tchamitchian, "The 'algorithme à trous'," in *Proc. of the International Workshop,* "Wavelets and Time Frequency Methods," Marseille, Dec 14–18, 1987, eds. J. M. Combes, A. Grossmann and Ph. Tchamitchian (Springer, 1989).

45. H. Elbrond Jensen, T. Hoholdt, and J. Justesen, "Double Series Representation of Bounded Signals," *IEEE Trans. Information Theory* **34** (1988), 613–624.

46. K. Wilson, "Generalized Wannier Functions," Cornell University, Physics Department, preprint, 1987.

47. D. J. Sullivan, J. J. Rehr, J. W. Wilkins, and K. G. Wilson, "Phase Space Wannier Functions in Electronic Structure Calculations," Cornell University, Physics Department, preprint, 1987.

48. I. Daubechies, S. Jaffard and J. L. Journé, "A Simple Wilson Basis with Exponential Decay," to appear in *SIAM J. Math. Anal.*

49. D. Esteban and G. Galand, "Application of Quadrature Mirror Filters to Split Band Voice Coding Schemes," *Proc. Int. Conf. Acoustics, Speech, and Signal Processing* (1977), 191–195.

50. M. J. Smith and D. P. Barnwell, "Exact Reconstruction for Tree-Structured Subband Coders," *IEEE Trans. Acoustics, Speech, and Signal Processing* **34** (1986), 434–441.

51. G. Beylkin, R. Coifman and V. Rokhlin, "Fast Wavelet Transforms and Numerical Algorithms, I," Mathematics Department, Yale University, preprint '89.